Cascaded numerical models for offshore floating wind turbines

Pegalajar Jurado, Antonio Manuel

Link to article, DOI:
10.11581/dtu:00000039

Publication date:
2019

Document Version
Publisher's PDF, also known as Version of record

Cascaded numerical models for offshore floating wind turbines

Antonio Pegalajar-Jurado

DTU Wind Energy PhD-0089(EN)
DOI number: 10.11581/dtu:00000039

September 2018

DTU Wind Energy
Department of Wind Energy

Authors: Antonio Pegalajar-Jurado

Title: Cascaded numerical models for offshore floating wind turbines

Department: Wind Energy

2018

Project Period:

September 15 2015 – September 14 2018

Education:

PhD

Supervisor:

Professor Henrik Bredmose

Co-supervisors:

Senior Scientist Robert Flemming Mikkelsen

DTU Wind Energy is a department of the Technical University of Denmark with a unique integration of research, education, innovation and public/private sector consulting in the field of wind energy. Our activities develop new opportunities and technology for the global and Danish exploitation of wind energy. Research focuses on key technical-scientific fields, which are central for the development, innovation and use of wind energy and provides the basis for advanced education.

DTU Wind Energy has a staff of approximately 240 and a further 35 PhD-students, spread across 38 different nationalities. The variety of research, education, innovation, testing and consultancy is reflected in the employment profile which includes faculty with research and teaching responsibilities, researchers and technical academic staff, highly skilled technicians and administrative staff.

Our facilities are situated at DTU Risø Campus and at DTU Lyngby Campus. Furthermore the department is running the national test stations in Høvsøre and Østerild.

Technical University of Denmark
Department of Wind Energy
Frederiksborgvej 399
Building 118
4000 Roskilde
Denmark

www.vindenergi.dtu.dk

TECHNICAL UNIVERSITY OF DENMARK

DOCTORAL THESIS

Cascaded numerical models for offshore floating wind turbines

Author:
Antonio PEGALAJAR-JURADO

Supervisors:
Henrik BREDMOSE
Robert F. MIKKELSEN

A thesis submitted in fulfillment of the requirements for the degree of Doctor of Philosophy

in the

Section of Fluid Mechanics
Department of Wind Energy

September 14, 2018

Abstract

Antonio PEGALAJAR-JURADO

Cascaded numerical models for offshore floating wind turbines

The aim of this doctoral thesis is to develop, investigate and validate numerical models for the dynamic analysis of floating offshore wind turbines.

The presented models address some of the challenges currently encountered in the design of floating substructures for offshore wind application. First, a state-of-the-art numerical model is set up and demonstrated in a wide range of environmental conditions with wind and waves. Second, this model is used to develop a simplified, efficient frequency-domain tool for the assessment of loads and response to wind and waves in the preliminary design phase. Third, a time-domain model is established and used to investigate the response of floating wind turbines to waves by comparing to experimental results.

The research focuses on aerodynamic and hydrodynamic loads, and how these can be efficiently combined with appropriate representations of the damping to yield a reasonable prediction of the response at low computational cost. The frequency-domain model includes aerodynamic and hydrodynamic loads and captures the main planar degrees of freedom of the floater, as well as tower deflection. The hydrodynamic damping is approximated analytically and the state-of-the-art model is used to extract the aerodynamic damping. The model is able to capture the dominant physics, while the reasons behind the most important deviations are identified. In the time-domain model only hydrodynamic loads are considered, including second-order inviscid slow-drift forces and viscous forces. The damping is identified from the experimental data using Operational Modal Analysis (OMA). The model generally reproduces well the response after proper damping calibration. The damping levels are observed to depend on the sea state and are found to be acceptably predicted by OMA for mild environmental conditions. For the larger sea states, the OMA-detected damping levels are found to deviate from the calibrated values.

The results show that good predictions can be obtained with both models. They also highlight the important role of damping in the dynamics of floating offshore wind turbines, and help to identify further research needs in this area.

Dansk Resumé

Antonio PEGALAJAR-JURADO

Multi-level numerisk modellering af flydende vindmøller

Formålet med nærværende ph.d. afhandling er at undersøge og validere numeriske modeller til dynamisk analyse af flydende vindmøller.

De udviklede modeller tager udgangspunkt i nuværende aktuelle udfordringer for design af flydere til offshore vindmøller. Først sættes en state-of-the-art model op for en flydende vindmølle og afprøves på en lang række kombinationer af vind og bølgetilstande. Modellen danner efterfølgende grundlag for en simplificeret og effektiv frekvensdomænemodel til vurdering af laster og respons for vind og bølger i prædesign fasen. Endelig udvikles en tidsdomænemodel til undersøgelse af bølgerespons. Modellen valideres mod eksperimentelle data.

Den fremlagte forskning fokuserer på aerodynamiske og hydrodynamiske laster og muligheden for at kombinere disse med en effektiv repræsentation af dæmpning for at opnå fornuftige responsværdier med en lav beregningsindsats. Frekvensdomænemodellen inkluderer aero- og hydro-dynamiske laster og beskriver de dominerende frihedsgrader for flyderens bevægelser i planen, inklusiv udbøjning af tårnet. Den hydrodynamiske dæmpning approksimeres analytisk og state-of-the-art modellen udnyttes til at parameterisere den aerodynamiske dæmpning. Modellen er i stand til at beskrive den væsentlige fysik altimens årsagerne til de vigtigste afvigelser fra state-of-the-art modellen identificeres. Tidsdomænemodellen begrænser sig til hydrodynamisk last og respons, inklusiv in-viskose lav-frekvente kræfter til anden orden og viskose kræfter. Dæmpningen estimeres ved hjælp af 'Operational Modal Analysis' (OMA). Modellen er generelt i stand til at genskabe det målte respons efter passende kalibrering. Det konstateres at dæmpningsniveauerne afhænger af sø-tilstanden og kan forudsiges med acceptabel nøjagtighed af OMA for små bølgehøjder. For større bølgehøjder afviger OMA-dæmpningsniveauerne fra værdierne opnået ved kalibrering.

Resultaterne viser at gode resultater kan opnås med begge modeller. De understreger den vigtige rolle af dæmpning for dynamikken af flydende vindmøller og peger herved mod nye forskningsbehov indenfor dette område.

Preface

The present thesis is divided into two parts. In Part I, an overview of the subject of floating offshore wind energy is given. First, wind energy and bottom-fixed offshore wind energy are briefly introduced including history, current status and expected projection. The emerging field of floating offshore wind is then presented in terms of dominant concepts, current projects, costs and challenges. An overview of the dynamics of floating wind turbines is also given, including theoretical background, numerical modelling, physical testing and validation. In Part II, three scientific papers are appended to the thesis in the following order:

Paper 1: Antonio Pegalajar-Jurado, Henrik Bredmose, Michael Borg, Jonas G. Straume, Trond Landbø, Håkon S. Andersen, Wei Yu, Kolja Müller and Frank Lemmer;
"State-of-the-art model for the LIFES50+ OO-Star Wind Floater Semi 10MW floating wind turbine", accepted for publication in *Journal of Physics: Conference Series*, 2018.

Paper 2: Antonio Pegalajar-Jurado, Michael Borg and Henrik Bredmose;
"An efficient frequency-domain model for quick load analysis of floating offshore wind turbines", accepted for publication in *Wind Energy Science*, 2018.

Paper 3: Antonio Pegalajar-Jurado and Henrik Bredmose;
"Reproduction of slow-drift motions of a floating wind turbine using second-order hydrodynamics and Operational Modal Analysis", submitted to *Marine Structures*, 2018.

September 14, 2018, Copenhagen
Antonio PEGALAJAR-JURADO

Acknowledgements

I would like to start by saying thank you to my main supervisor Professor Henrik Bredmose for the opportunity to pursue this project, which allowed me to spend three years learning about the exciting world of floating offshore wind turbines. I am also grateful for all the engaging discussions we have had together, and for all the constructive criticism you provided on my work. On the human side, you are also a funny, modest and accessible person that one can feel comfortable talking to. My co-supervisor Senior Scientist Robert F. Mikkelsen is also thanked for his craftsmanship and lab experience, which came in handy during the physical tests of floating wind turbines I was involved in. Also deserves my gratitude former Postdoc Michael Borg, with whom I extensively collaborated, and from whom I also learned a great deal.

My research visit to the National Renewable Energy Laboratory (NREL) in Boulder (Colorado) was possible thanks to Senior Researcher Amy Robertson, Senior Engineer Jason Jonkman and Software Engineer Greg Hayman. I thank them for the opportunity and for the good interactions we had during my three months there. I am thankful to the LIFES50+ project and the Technical University of Denmark (DTU), the two financial supporters of my scholarship.

To my colleagues at the Fluid Mechanics Section of DTU Wind Energy, for making work a bit more enjoyable. A special mention goes to Amin Ghadirian, with whom I had countless discussions on hydrodynamics, but also on e-bikes, movies, restaurants, and even sometimes Elon Musk. The Section Secretary, Marianne H. Arbirk, may be one of the most efficient persons I have ever met, and she deserves to be acknowledged too for making my life easier.

Last but not least, I would like to say thank you to my friends, my parents Ana María and Ildefonso, my sister Dori, and my girlfriend Hanna. They provided inexhaustible moral support, as crucial for this journey as the very hands that are typing these words.

September 14, 2018, Copenhagen
Antonio PEGALAJAR-JURADO

"Engineering is the art of modelling materials we do not wholly understand, into shapes we cannot precisely analyze, so as to withstand forces we cannot properly assess, in such a way that the public has no reason to suspect the extent of our ignorance."

- Dr. A. R. DYKES

Contents

Part I

Overview

Chapter 1

Introduction

1.1 Wind energy

The power in the wind has been harnessed by humans for thousands of years. The first known application of wind dates from 5000 BC in Mesopotamia, where sailing boats are known to have traveled from the Tigris-Euphrates Delta to Oman and Northwest India [1]. Later, around 600 AD, windmills like the ones shown in Fig. 1.1 started being used in Europe to mill grain and pump water [2].

FIGURE 1.1: Windmills in the Netherlands. Photo from [3].

In the end of the nineteenth century, once electrical generators had been invented and some basic developments in aerodynamics had been made, windmills started being applied to electrical power generation. James Blyth was the first person to produce electricity using wind power in Glasgow (UK) in 1887, followed by Charles

Brush (Cleveland, Ohio, 1888) and Poul la Cour (Askov, Denmark, 1891) [2]. However, the general interest in wind energy declined after the First World War due to cheaper fossil fuels. It was not until the 1970s, due to the first global oil crisis of 1973, that the modern wind energy industry was born. Back then, most governments interested in wind energy (such as the UK, Germany, the US and Canada) supported the development of large turbines by big companies, while Denmark opted for small turbines developed by small companies and wind energy pioneers [4]. Since the construction of the first modern wind turbines in the late 1970s the wind industry has matured significantly, and today's state-of-the-art wind turbines (see Fig. 1.2) come with rated powers up to 10 MW, which can provide clean electricity to more than 8000 households [5].

FIGURE 1.2: Today's wind turbines are typically horizontal-axis, three-bladed machines. Photo from [3].

Although wind energy deployment started in Europe and North America the market is expanding rapidly to other areas of the world, supported by favorable energy policies, impulsed by cost reductions, and with the consequent need to adapt to different climate conditions, cultural aspects and infrastructure levels. As of 2017, wind energy provided 4% of the global electricity production. If the current growth rate continues, wind could supply up to 30% of the world's electricity consumption by 2030 [5]. In the European Union, leaders have committed to reaching at least 27% share of renewable energy by 2030 [6]. In Denmark, the share of wind power in the total electricity production in 2017 is close to 50%, a goal that the Danish government intends to reach by 2020. Furthermore, onshore wind power — which represented more than 95% of the installed wind capacity worldwide in 2017 — has seen an important reduction in the levelized cost of energy (LCOE) in recent years and is now subsidy-free in several markets [5].

1.2 Bottom-fixed offshore wind energy

Offshore wind energy is the deployment of wind power in bodies of water, normally in the sea. There are several reasons to install wind turbines offshore, with the most important being:

- Winds are stronger and steadier over the sea, which is directly translated into higher energy yields and lower fatigue loads on the mechanical components, due to lower turbulence.
- The acoustic and visual impacts are smaller, which circumvents some problems related to social acceptance that onshore wind deployment often encounters when wind turbines are erected near populated areas.
- There is more space available offshore, which allows for larger separation between turbines and reduced wake effects.
- Larger turbines can be used offshore, since transport by sea is virtually only limited by the vessel size.

Bottom-fixed offshore wind turbines are rigidly connected to the seabed. There are three main types of bottom-fixed support structures for wind turbines: monopiles, gravity-based foundations and jackets. The connection to the wind turbine tower is usually made with a transition piece, while the connection to the seabed can rely on gravity, penetration of the pile into the seabed, or suction buckets. The majority of the the offshore wind farms in Europe use monopiles as support structures with 82% of the market share by 2017, followed by jackets and gravity-based foundations [7].

Offshore bottom-fixed wind farms have been commercial since 1991, when the first large offshore wind farm was installed 2.5 km off the coast of Vindeby (Denmark) [2]. Vindeby wind farm, with eleven Bonus 450 kW wind turbines mounted on gravity-based foundations, was decommisioned in 2017. Although onshore wind still represents the vast majority of wind power, offshore wind has also seen an important expansion during Vindeby's lifetime, especially in Europe [8]. At the end of 2017, Europe had a total of 15.8 GW of installed offshore wind capacity with a total of 4149 wind turbines, most of them in the North Sea. About 20% of this total capacity was installed and connected in 2017 alone, corresponding to 3.1 GW and 560 turbines with an average rated power of 5.9 MW [7]. Given the rapid growth seen in recent years, the total installed capacity in Europe is expected to grow to 25 GW by 2020 (see Fig. 1.3).

Costwise, in the past few years the LCOE for offshore wind has decreased significantly, exceeding the predictions of experts and even with subsidy-free bids in European tenders for offshore wind farms planned for 2024 and later [5]. The current offshore wind market is characterized by a trend towards bigger turbines and deeper waters, with monopiles being installed in water depths up to 35 m, while jacket foundations can be found in waters up to 60 m deep. New technology developments are continuously making the feasible depth range larger. However, the vast majority of the world's oceans are significantly deeper, and the regions where

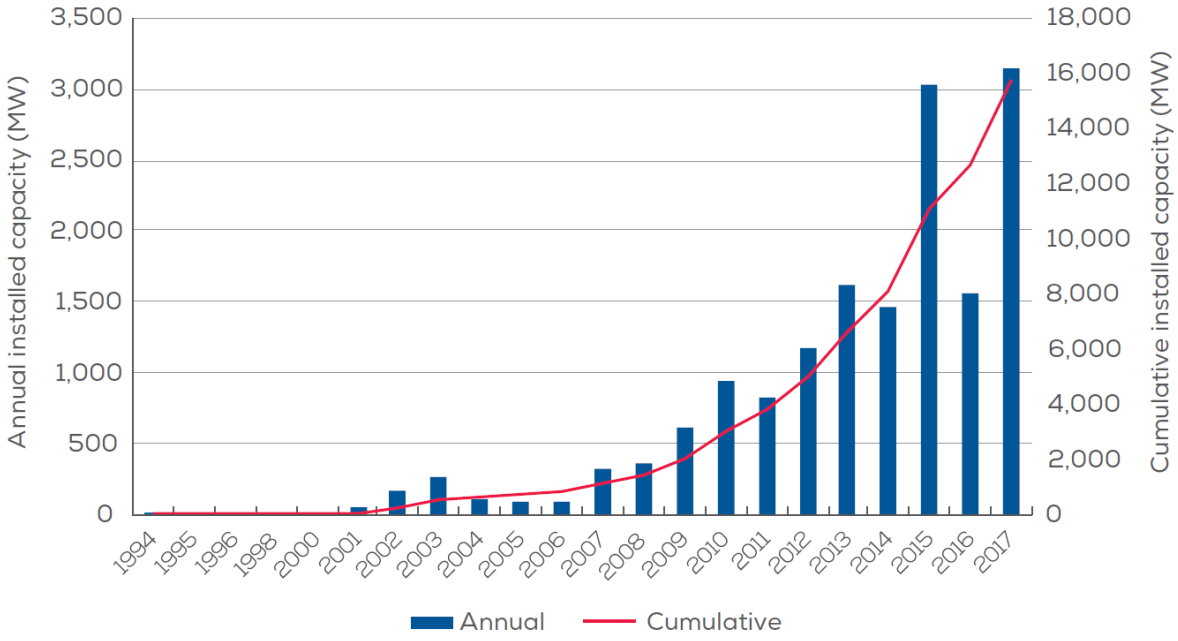

FIGURE 1.3: Annual and cumulative installation of offshore wind power in Europe [6].

the water depths are too large for bottom-fixed foundations are pursuing floating alternatives, which are expected to become increasingly feasible in the coming years.

1.3 Floating offshore wind energy

In Europe, 80% of the offshore wind resources are located in water depths of 60 m or deeper [6]. Hence, the offshore wind industry is now mimicking the tendency seen in the oil and gas industry, when platforms moved from fixed to floating to gain access to deep water sites [9]. When compared to bottom-fixed offshore wind, floating offshore wind power has a series of advantages:

- Even stronger and steadier winds.
- Even smaller acoustic and visual impacts.
- Even more space is available in deep waters.
- Floating wind can be installed where bottom-fixed offshore wind is not feasible due to bathymetry constraints.
- Floating wind turbines are easier to remove, relocate and decommission, since most concepts can be towed.
- The cost of floating substructures is less sensitive to local site constraints (e.g. water depth) than that of bottom-fixed foundations, since only the cost of the mooring system depends directly on these.

Floating and bottom-fixed offshore wind are thus complementary technologies, which can mutually benefit in terms of supply chain, operation and maintenance (O&M)

and ancillary services. In addition, since bottom-fixed is already an industrialized technology, floating wind can also benefit from it in terms of research and technology development in its transition towards industrialization.

1.3.1 Types of floating substructures

A floating substructure for offshore wind includes the floater (for buoyancy and structural purposes), the mooring and anchor systems (for station-keeping) and the dynamic power cable (for grid connection). Although many concepts exist today, they are usually classified by the means they maintain stability when the aerodynamic thrust on the wind turbine creates an overturning moment. The main types of floating substructures are shown in Fig. 1.4 and described below:

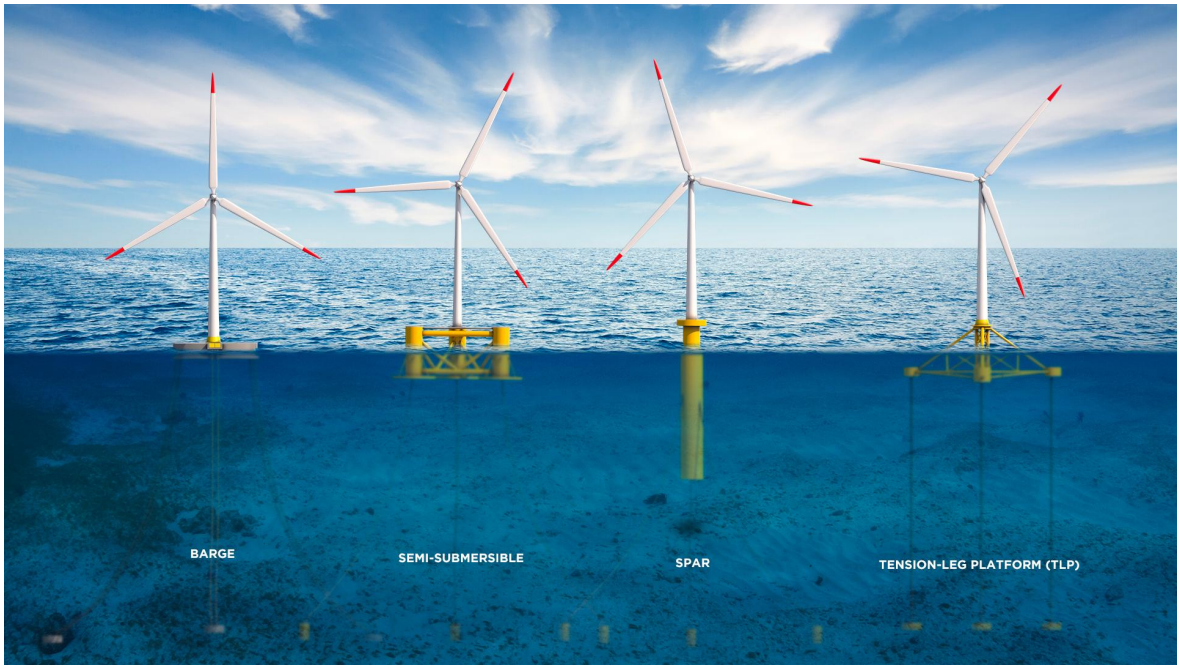

FIGURE 1.4: Types of floating substructures for offshore wind. Illustration from [6].

Semi-submersibles or semisubs are buoyancy-stabilized floaters. Since they have shallow draft, they are suitable for a wide variety of site conditions and easy to transport and install. Generally they are heavy and complex to manufacture.

Spar buoys or spars are ballast-stabilized, simpler floaters, which makes them easier to manufacture. Their deeper draft limits their applicability to certain sites and introduces some challenges in transportation and assembly.

Tension-leg platforms (TLPs) are mooring-stabilized by a set of taut lines, which reduces the floater motions but also introduces higher demands on mooring design and soil conditions. On the other hand, they have shallow draft and low weight.

Barges are also buoyancy-stabilized floaters with the shallowest draft of all four types, which makes them easy to install. They usually experience larger motions, hence they sometimes have moon pools to provide additional damping.

The mooring lines are typically chains, metallic wires or synthetic ropes, commonly attached to the seabed through drag anchors, suction buckets or gravity anchors. Semisubs, spars and barges are moored with catenary lines and normally use drag anchors. On the other hand, TLPs use taut lines for station-keeping and stability, connected to the seabed by suction buckets or gravity anchors.

1.3.2 Current projects

The total floating offshore wind capacity installed globally amounts to 50 MW as of 2018, mainly in Europe and Japan (see Tab. 1.1). Most of these demonstrators are single prototypes, with the exception of Hywind Scotland as the world's first floating offshore wind farm (see Fig. 1.5), commissioned in 2017 off the coast of Peterhead, Scotland. The wind farm, comprised of five Siemens-Gamesa 6 MW wind turbines mounted on Hywind spar-buoy floaters, has already reached average capacity factors around 65% for its first three months of operation [10].

First power	Country	Project	Total capacity	Turbine rating	Project developer	Technology developer	Concept	Turbine supplier
2009	Norway	Hywind I	2.3 MW	2.3 MW	Statoil	Statoil	Hywind	Siemens
2011	Portugal	WindFloat Atlantic Phase 1*	2 MW	2 MW	EDPR, Repsol, Chiyoda, Mitsubishi	Principle Power	WindFloat	Vestas
2013	Japan	Kabashima	2 MW	2 MW	Toda Corporation	Toda Corporation	Hybrid spar	Hitachi
2013	Japan	Fukushima FORWARD	2 MW	2 MW	Marubeni	Mitsui Engineering & Shipbuilding	Semi-Sub	Hitachi
2015	Japan	Fukushima FORWARD	7 MW	7 MW	Marubeni	Mitsubishi Heavy Industries	V-Shape Semi-Sub	MHI
2016	Japan	Fukushima FORWARD	5 MW	5 MW	Marubeni	Japan Marine United	Advanced Spar	Hitachi
2017	UK	Hywind Pilot Park	30 MW	6 MW	Statoil	Statoil	Hywind	Siemens
2018	France	FloatGen	2 MW	2 MW	IDEOL	IDEOL	Damping Pool	Vestas

** WindFloat 1 decommissioned in 2016. The WindFloat 1 substructure will be redeployed in the Kincardine pre-commercial project in Scotland.*

TABLE 1.1: Commissioned floating offshore wind projects [10].

These commissioned projects and new ones to come are expected to demonstrate technological and economical feasibility, setting the scene for the large-scale deployment of floating offshore wind power expected in the next decade in Europe, East Asia and North America [10].

1.3.3 Maturity of technology

For many years, floating offshore wind has been confined to research and development (R&D). However, the technology has rapidly developed in recent years, and it is now moving towards industrialization. The semisub and spar concepts have already reached a technology readiness level (TRL) above 8 [6]. Figure 1.6 shows the evolution of TRL for different floating concepts.

FIGURE 1.5: Hywind Scotland floating offshore wind farm. Photo by Øyvind Gravås/Woldcam/Equinor [11].

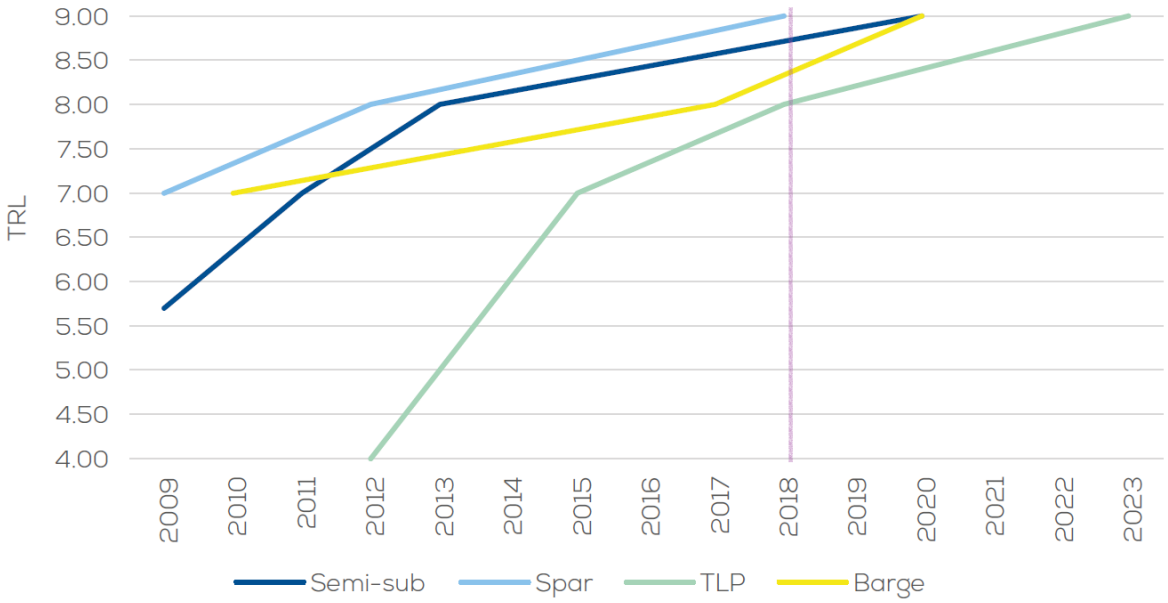

FIGURE 1.6: Technology readiness level (TRL) of floating offshore wind substructures [6].

1.3.4 Costs

Now that the three "realms" of wind energy have been introduced, they can be analyzed together in terms of expected cost evolution. The International Energy Agency (IEA) published in 2016 a study forecasting the costs and cost drivers for onshore, bottom-fixed offshore and floating offshore wind [8]. The main message from the experts is that the LCOE of wind power is expected to continuously drop in the next

30 years (see Fig. 1.7). It is believed that onshore wind will remain more competitive than offshore, and bottom-fixed offshore more competitive than floating. On the other hand, offshore wind would experience greater absolute reductions in LCOE, although with a higher level of uncertainty. Within offshore, the difference between bottom-fixed and floating wind would narrow over time, especially between 2020 and 2030.

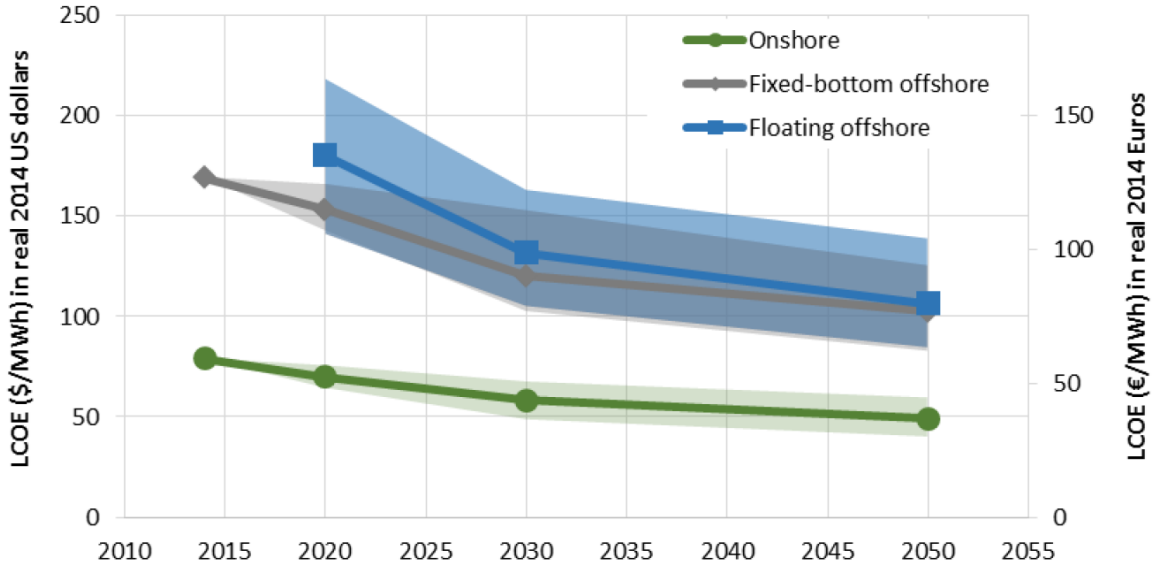

FIGURE 1.7: Expert estimates of median-scenario levelized cost of energy (LCOE) for all three wind applications [8]. The markers indicate the median expert estimates, whereas the shaded areas show the 1st-3rd quartiles.

The main cost drivers for these cost reductions are also listed in [8]. For onshore wind, improvements in capacity factor (larger rotor diameters, more efficient designs and higher hub heights) and savings in capital expenditure (CapEx) are thought to be the main drivers of LCOE reductions. For fixed-bottom offshore wind, however, capacity factors would not play such an important role, and the reductions in LCOE are expected to be due to CapEx reductions and improvements in financing costs. Finally, the main driver of LCOE reductions for floating offshore wind is linked to improvements in the capacity factor, due to the belief that only floating wind can reach deeper water locations with stronger and steadier winds. Here, importance is also given to foundations and support structures, as well as to wind turbine installation.

1.3.5 Challenges

The development of the bottom-fixed offshore wind sector is strongly linked to the North Sea: a shallow basin with relatively uniform site conditions, shared by countries willing to decarbonize their energy systems [12]. On the other hand, the development of floating offshore wind needs to be supported by countries for which onshore wind, bottom-fixed offshore wind or solar energy is not sufficient to meet the energy demand, or simply not an option. At the same time, these countries need

to have the necessary investment and energy planning policies for the development to happen. As most development projects will require government support in form of funding, the political risk is considerable in many markets [9]. These potential markets are Japan, South Korea, US, UK, Portugal, Spain, France and the Mediterranean Sea, among others.

In addition to these political and investment sensitivities, the deployment of floating offshore wind in a commercial scale is associated with a number of technical challenges. According to [5] one of the research areas that require significant efforts to meet the industry's needs is modelling of floating wind power systems, including wind turbine, floating substructure and mooring system. A more detailed list of the most important long-term challenges for floating offshore wind was given by the European Academy of Wind Energy (EAWE) in 2016 [4]. In terms of hydrodynamics and response, the main challenge is to improve the numerical prediction of wave-structure interaction. The hydrodynamic modelling of floating wind turbines is usually based on potential flow, which neglects viscous effects. The accurate prediction of viscous loads on complex floating structures with sharp edges is still an ongoing effort. In addition, linear wave theory is often used to describe the incident wave field, although ocean waves are generally nonlinear even in deep water. It is still unclear how important nonlinear wave loads are for the dynamics of the system, or under what environmental conditions they need to be accounted for. Computational fluid dynamics (CFD) models can capture all nonlinear hydrodynamic effects including breaking waves and green water, but they remain computationally expensive and not always accurate. Validation of numerical models against physical test data is the most reliable way to assess their performance, but studies on full-scale validation of numerical tools for the response of floating wind turbines to wind, waves and current are scarce or non-existent. Although several studies exist on validation against lab-scale data, it is always a challenge to correctly scale the aerodynamic loads in the laboratory. Another challenge mentioned in [4] is to develop integrated tools and methods for robust design and optimization of offshore floating wind turbines. While current design practices are often based on experience, there is a need for efficient and robust simplified tools that can be used for design optimization, and that take into account all the subsystems that influence the global system response.

Additional technical challenges have been recently identified by the Floating Wind Joint Industry Project (JIP) [10], mainly related to electrical systems (dynamic power cables and floating substations), mooring systems (reduction in fatigue and failure probability, complex installation, new materials, designs for shallow water) and infrastructure and logistics (constraints related to existing port facilities and vessels, O&M strategies). Finally, floating offshore wind also opens new questions in other wind energy fields such as aerodynamics (wake effects and turbulence), control and environmental and social impact.

1.4 Motivation and thesis structure

In a fast world with a growing population, further development of the floating offshore wind industry will play an important role in the transition to clean energy and the battle against climate change. The information presented in this chapter can be summarized in three main points: i) offshore wind power is expanding at an accelerating rate and it will be an important contributor to the decarbonization of the actual energy system; ii) the expansion is mainly driven by ever-decreasing costs associated to technology maturement; and iii) a number of challenges must be addressed in order to meet the desired scenario.

The research presented in this thesis addresses some of the technical challenges introduced in Section 1.3.5, more precisely two of them: i) efficient and robust simplified tools that can be used for design optimization; and ii) modelling of wave-structure interaction and validation against physical test data. The former is addressed with the development of an efficient frequency-domain model (Paper 2) and its validation against a time-domain, state-of-the-art model (Paper 1). The latter entails the development of a time-domain model (Paper 3) including nonlinear hydrodynamics and identification of viscous damping, and its validation against physical test results.

The rest of this thesis has been structured as follows:

- Chapter 2 gives an overview of the dynamics of floating wind turbines including the loads involved, the different options to model them numerically, and an introduction to physical testing and validation.
- Chapter 3 provides a summary of Part II, which contains three scientific papers addressing the aforementioned challenges in the topic of numerical modelling of offshore floating wind turbines.

References

[1] D.T. SWIFT-HOOK. "History of wind power". In: *Comprehensive renewable energy*. Elsevier Ltd, 2012, pp. 41–72.

[2] J. BEURSKENS. "The history of wind energy". In: *Understanding wind power technology: Theory, deployment and optimisation*. Wiley Blackwell, 2014, pp. 1–44.

[3] *Pexels*. URL: https://www.pexels.com/.

[4] G. van KUIK and J. PEINKE, eds. *Long-term research challenges in wind energy - A research agenda by the European Academy of Wind Energy*. Springer, 2016.

[5] C. AABO, P.H. JENSEN, M. ANDERSSON, J.S. HOLM, and E.L. NIELSEN. *Annual research and innovation agenda*. Tech. rep. Megavind, 2017.

[6] *Floating offshore wind vision statement*. Tech. rep. WindEurope, 2017.

[7] T. REMY and A. MBISTROVA. *Offshore wind in Europe: Key trends and statistics 2017*. Tech. rep. WindEurope, 2018.

[8] R. WISER, K. JENNI, J. SEEL, E. BAKER, M. HAND, E. LANTZ, and A. SMITH. *Forecasting wind energy costs & cost drivers - The views of the world's leading experts*. Tech. rep. IEA Wind Task 26, 2016.

[9] J. CRUZ and M. ATCHESON, eds. *Floating offshore wind energy - The next generation of wind energy*. Springer, 2016.

[10] R. JAMES, W.Y. WENG, C. SPRADBERY, J. JONES, D. MATHA, A. MITZLAFF, R.V. AHILAN, M. FRAMPTON, and M. LOPES. *Floating Wind Joint Industry Project - Phase I Summary Report: Key findings from electrical systems, mooring systems, and infrastructure & logistics studies*. Tech. rep. Carbon Trust, 2018.

[11] *Equinor ASA*. URL: https://www.equinor.com/.

[12] M. GUZZETTI. *Floating offshore wind (part 1): Coming of age*. 2017. URL: https://green-giraffe.eu/blog/floating-offshore-wind-coming-age.

Chapter 2

Dynamics of floating offshore wind turbines

2.1 Loads on a floating wind turbine

Floating wind turbines are deployed in deep water, which sometimes corresponds to several kilometers offshore. The loads they are exposed to are mainly due to the wind and the marine environment, as shown in Fig. 2.1. In general, the loads can be divided into:

- aerodynamic loads on the wind turbine rotor, nacelle and tower;
- hydrodynamic loads on the floater and mooring lines due to waves, current and tides;
- other environmental loads such as icing, earthquakes and lightnings;
- gravitational loads due to weight and marine growth;
- turbine-induced loads related to tower shadow, generator torque and controller effects;
- internal loads due to structural flexibility;
- and mooring loads from the station-keeping system.

The most important loads — related to structural response, aerodynamics, hydrodynamics and mooring system — for a given design are assessed during the design process with the aid of numerical and experimental methods. Both numerical simulations and experimental tests provide valuable insights into the performance and feasibility of the floating wind turbine under consideration. However, although modelling and testing are in principle straightforward, the Engineering challenge is to combine the two in a rational way.

2.2 Numerical methods

A good amount of experience from the oil & gas industry has been readily incorporated into floating offshore wind technology. However, in general floating offshore

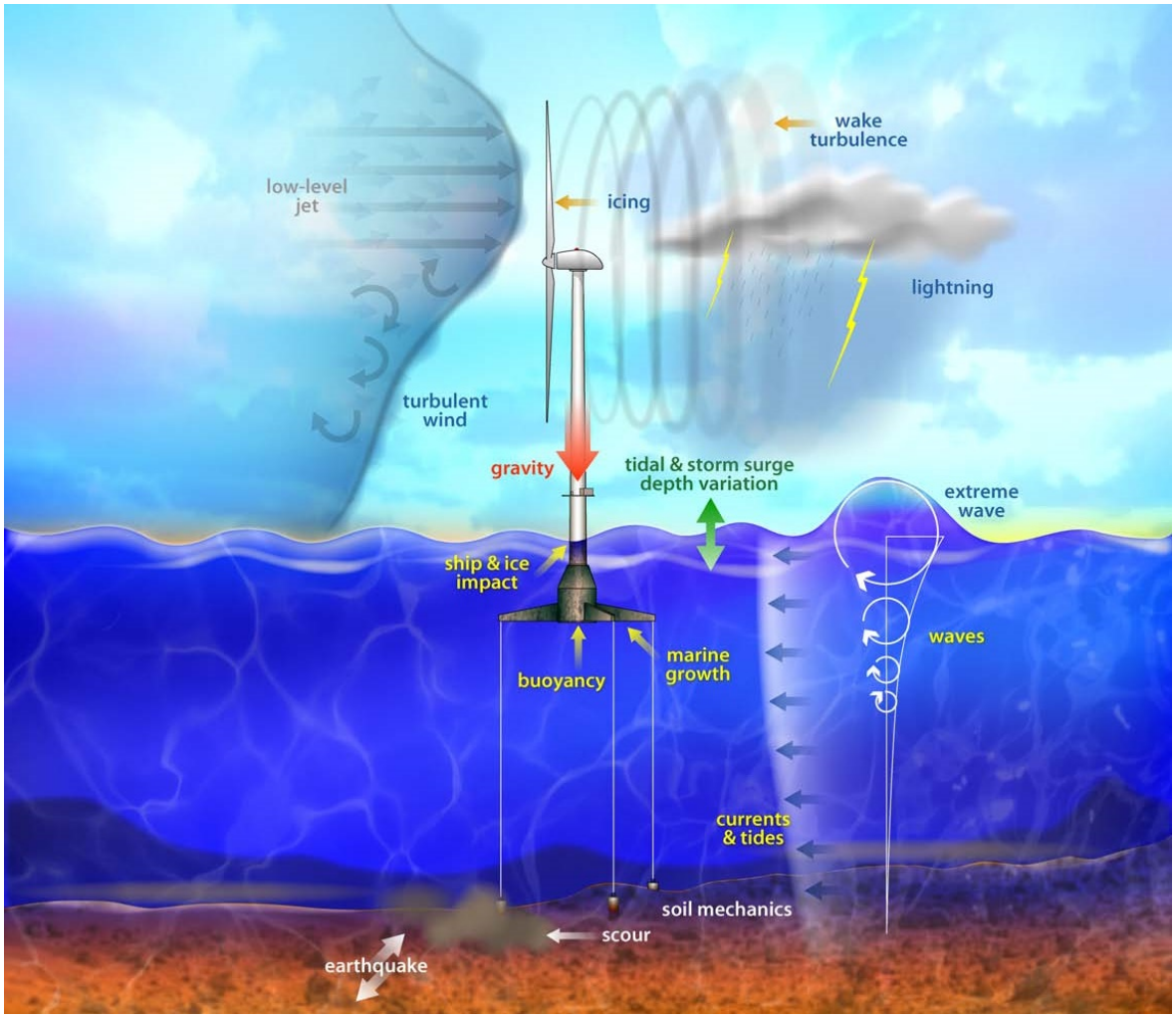

FIGURE 2.1: Loads on a floating offshore wind turbine [1].

wind turbines experience more dynamic conditions than an offshore platform for oil & gas. The floaters employed for offshore wind are usually smaller, and support highly flexible structures that withstand strong aerodynamic loads applied at high altitudes. In addition, the wind turbine controller has a significant impact on the floater motion (see, for example, [2]). On the other hand, the designers of floating substructures for offshore wind aim at minimizing the wind turbine static displacement (heel angle) and motion (nacelle acceleration) to comply with limits for safe wind turbine operation. The combination of increased dynamic complexity and stricter design requirements puts more demand on the design process of a floating offshore wind turbine.

Ideally, the whole wind turbine lifetime should be simulated in high-fidelity numerical tools. In practice, using CFD (computational fluid dynamics) and FEM (finite-element methods) to calculate the detailed aerodynamic loads and elastic response of a rotor for its entire lifetime would take longer than the lifetime itself [3]. If the wind turbine is mounted on a floating substructure, hydrodynamic loads and mooring cables would further increase the complexity of such demanding simulations.

A realistic alternative is to condense the key physical phenomena and observed experience into models suitable for design and analysis. These models, which cover a wide range of accuracy and computational cost levels, need to be validated against physical experiments or higher-fidelity models. The whole cascade of models ranging from fast, simplified tools to full-scale physical tests is shown in Fig. 2.2. Here the concept of *cascade* is used in two ways. First, the different steps or levels in a cascade represent the different levels of model fidelity. Second, the flow from the upper to the lower levels represents the process of extracting information from a model and including it into a simpler one, or *cascading*.

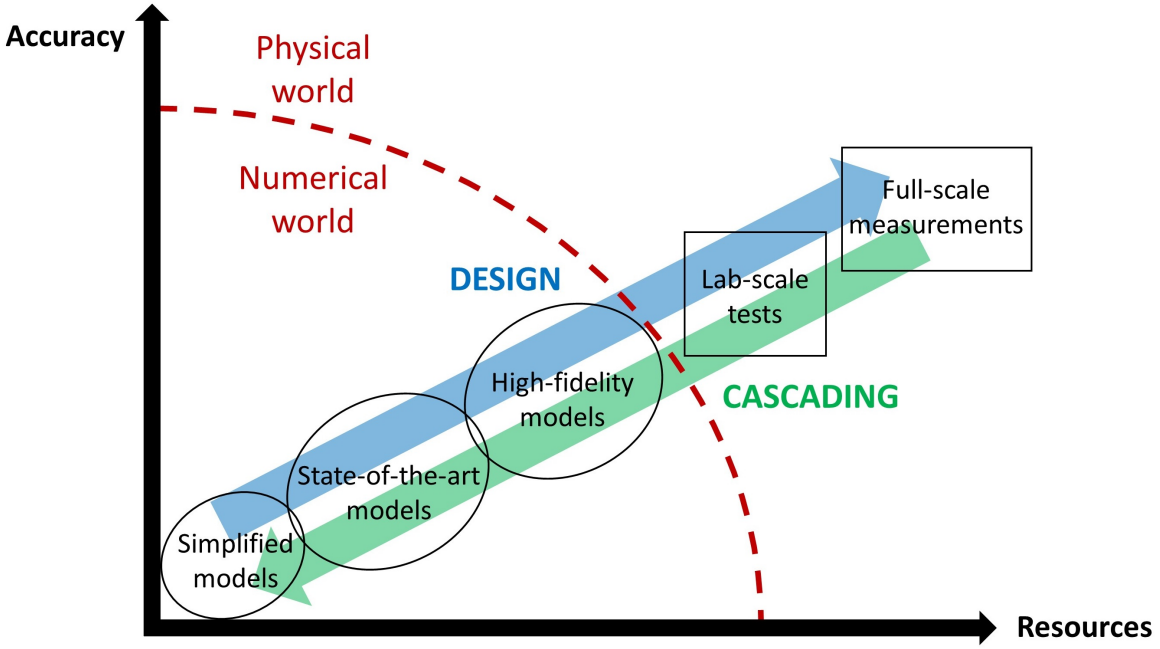

FIGURE 2.2: Cascade of models.

In the design of a floating substructure for an offshore wind turbine, different stages of the design require different tools. Thus, the different ways of representing the physical system are complementary, as shown in Fig. 2.2. Simplified, frequency-domain numerical tools are useful to explore several designs in the first stages of the design process, while state-of-the-art coupled models should be employed to assess the performance of the optimal design over a wide range of environmental conditions. If needed, detailed analysis at component level can be carried out in high-fidelity numerical models. On the physical side, laboratory-scale tests can serve as a benchmark for model validation and as proof-of-concept, while a full-scale physical prototype is normally used for demonstration and further validation of the numerical tools.

As mentioned in the previous section, the dynamics of floating offshore wind turbines mainly depends on four elements: structural dynamics, aerodynamics, hydrodynamics and mooring dynamics. Since each of these elements can be modelled with different levels of fidelity, the rest of this section provides an introduction to the different modelling options in each case, as well as an overview of the most

widely used numerical models that allow fully coupled dynamic simulations: the aero-hydro-servo-elastic codes.

2.2.1 Structural dynamics

The simplest dynamic structural model of a floating offshore wind turbine is a rigid body with the six degrees of freedom (DoFs) shown in Fig. 2.3: translations surge, sway and heave; and rotations roll, pitch and yaw. The generic equations of motion (EoM) follow from Newton's second law, and can be written in matrix form as

$$\mathbf{M}\ddot{\boldsymbol{\xi}} + \mathbf{G}(\dot{\boldsymbol{\xi}})\dot{\boldsymbol{\xi}} = \mathbf{F}, \tag{2.1}$$

where $\boldsymbol{\xi} = [\xi_1 ... \xi_6]^T$ is the 6x1 vector of displacement in the six DoFs, dot indicates differentiation with respect to time, $\mathbf{M}$ is the 6x6 rigid-body mass and inertia matrix, $\mathbf{G}(\dot{\boldsymbol{\xi}})$ is the matrix of rigid-body Coriolis and centripetal forces, and the 6x1 vector $\mathbf{F}$ represents the external forces and moments. The Coriolis and centripetal term is due to the rotation of the body coordinate system with respect to the inertial coordinate system (Fossen [4]), and makes the equation nonlinear. Under the assumption of small rotations, Eqn. (2.1) can be linearized to give

$$\mathbf{M}\ddot{\boldsymbol{\xi}} = \mathbf{F}_{aero} + \mathbf{F}_{hydro} + \mathbf{F}_{moor}, \tag{2.2}$$

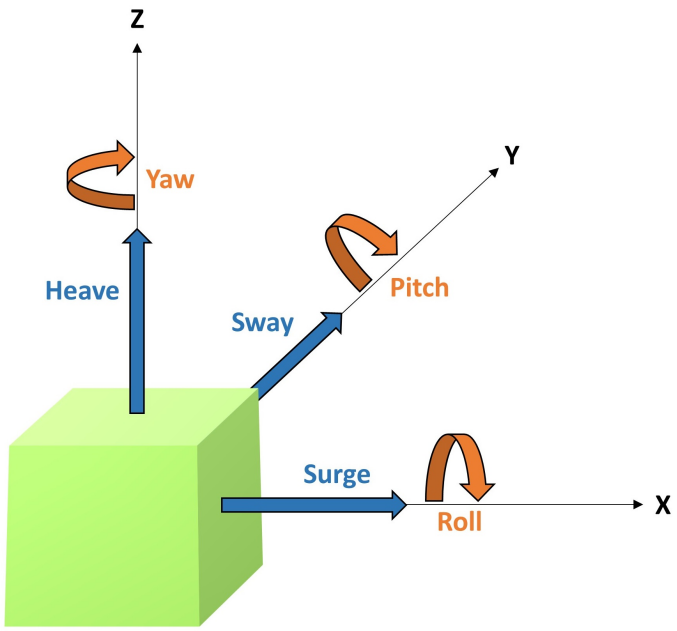

FIGURE 2.3: Rigid motion of a floating body in six degrees of freedom.

where the load vector $\mathbf{F}$ is now divided into aerodynamic, hydrodynamic and mooring loads acting on the system. Some of the right-hand side forces and moments in

Eqn. (2.2) that depend on position, velocity or acceleration can be linearized and partially or completely moved to the left-hand side:

$$(\mathbf{M}+\mathbf{A})\ddot{\boldsymbol{\xi}}+\mathbf{B}\dot{\boldsymbol{\xi}}+\mathbf{C}\boldsymbol{\xi}=\mathbf{F}_{aero}+\mathbf{F}_{hydro'}. \tag{2.3}$$

Here some hydrodynamic effects represented by $\mathbf{F}_{hydro}$ in Eqn. (2.2) have been moved to the left-hand side by augmenting the mass matrix with an added mass matrix $\mathbf{A}$, and by introducing a damping matrix $\mathbf{B}$ and a restoring matrix $\mathbf{C}$ that includes linear hydrostatic and mooring restoring effects. This way $\mathbf{F}_{hydro'}$ only contains the wave excitation loads (which do not depend on the body motions in a linear analysis), as well as nonlinear hydrostatic, radiation and viscous effects.

Although rigid-body models are useful to represent the global motion of a floating wind turbine, flexibility needs to be included in certain cases. A way of including flexibility of some elements while keeping the problem relatively simple is using modal dynamics. In modal analysis the deformation of a structure is approximated by a linear combination of predefined mode shapes, reducing the complexity of the problem to a few DoFs. The use of modal analysis is illustrated here by applying it to the beam with a top mass shown in Fig. 2.4, which could represent an onshore wind turbine tower with height-dependent mass and stiffness properties $m(z)$ and $EI(z)$ and no damping. The beam is subjected to a height- and time-dependent load $p(z,t)$, causing a time-dependent deflection $v(z,t)$ governed by the Euler-Bernoulli dynamic beam equation

$$m\ddot{v}+(EIv_{zz})_{zz}=p, \tag{2.4}$$

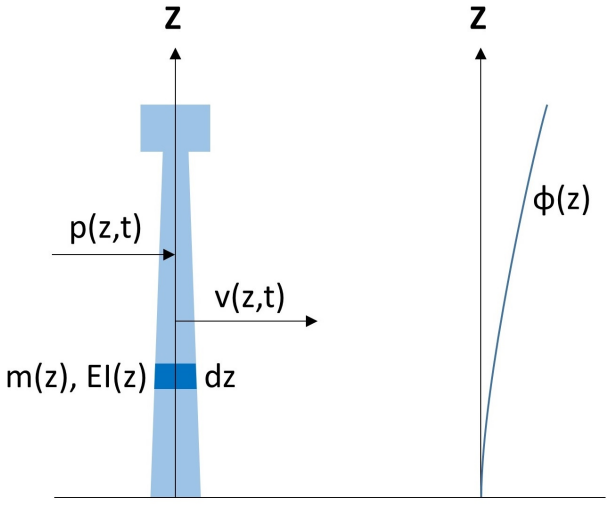

FIGURE 2.4: Modal representation of an onshore wind turbine tower.

where the subindex $_{zz}$ indicates partial differentiation with respect to z twice. In case of no external loading, we have $p=0$ and the beam vibrates freely at certain eigenfrequencies associated to specific mode shapes. It can be shown through Sturm-Liouville theory that the modal shapes are orthogonal and make out a complete

basis for the deflection. Thus, one can write the deflection as a linear combination of infinite mode shapes ϕ_i and modal coefficients γ_i,

$$v(z,t) = \sum_{i=1}^{\infty} \phi_i(z)\gamma_i(t). \tag{2.5}$$

Usually the relevant modes are those with a natural frequency within the range of forcing frequencies. Hence, in practice only a few modes are employed for the modal expansion. In this example we use only the first mode shown in Fig. 2.4, hence $v(z,t) = \phi_1(z)\gamma_1(t)$. Inserting this into Eq. (2.4), multiplying by ϕ_1, integrating along the beam and applying orthogonality leads to

$$\ddot{\gamma}\int_z m\phi_1^2 dz + \gamma\int_z EI\phi_{1,zz}^2 dz = \int_z p\phi_1 dz \quad \Longrightarrow \quad m_g\ddot{\gamma} + k_g\gamma = f_g, \tag{2.6}$$

where m_g, k_g and f_g are generalized mass, stiffness and force, respectively. Equation (2.6) is an ordinary second-order differential equation, much easier to solve than the fourth-order partial differential equation (2.4).

Although only one mode has been considered here, a better representation of the structural response can be obtained if more modes are included in the analysis. The number of independent equations to solve is the same as the number of modes considered, hence a reasonable balance between accuracy and computational cost must be sought. An important consideration is that modal analysis can only capture the modes chosen to represent the structure, and they need to be computed in advance. Other shapes than eigenshapes can be used, but then orthogonality is lost. Further details on modal analysis of marine structures can be found in, for example, Naess and Moan [5] and the references therein.

Alternatively, a more detailed structural model of the floating wind turbine or of any of its components can be obtained with FEM (which discretizes the structure into finite elements that represent its mass, damping and stiffness properties) combined with the multibody formulation. Further details on these methods can be found in books such as Cook et al. [6] and Shabana [7].

2.2.2 Aerodynamics

The simplest aerodynamic representation of a wind turbine is the 1-D momentum theory, which models the rotor as a permeable ideal disc slowing down the wind flow. This model, also referred to as actuator point, provides simple relationships between the undisturbed velocity V_∞ and the thrust T and aerodynamic power P,

$$T = \frac{1}{2}\rho C_T A V_\infty^2, \tag{2.7}$$

$$P = \frac{1}{2}\rho C_P A V_\infty^3. \tag{2.8}$$

Here ρ is the air density, A is the area swept by the rotor and C_T and C_P are the thrust and power coefficients, respectively. The two coefficients depend on the axial induction factor a, which relates the velocity at the rotor plane u with the upstream velocity through $u = V_\infty(1-a)$. The maximum power coefficient achievable by an ideal wind turbine is $C_{P,max} = 16/27 \approx 0.59$, known as the Betz limit.

The blade element momentum (BEM) method, developed by Glauert [8], combines momentum theory with local blade element information into a 2-D method to calculate steady thrust and power for a given wind turbine configuration. Figure 2.5 shows the cross-section at a radial position r of a wind turbine blade pointing upwards while rotating clockwise with an angular velocity ω. The airfoil sees a relative velocity caused by the incoming wind speed V_∞, its own rotation ωr, and the induced wind given by the axial and tangential induction factors, a and a'. The magnitude of the relative velocity V_{rel} and its angle with the rotor plane ϕ (inflow angle) are given as

$$V_{rel} = \sqrt{(V_\infty(1-a))^2 + (\omega r(1+a'))^2}, \tag{2.9}$$

$$\tan\phi = \frac{V_\infty(1-a)}{\omega r(1+a')}. \tag{2.10}$$

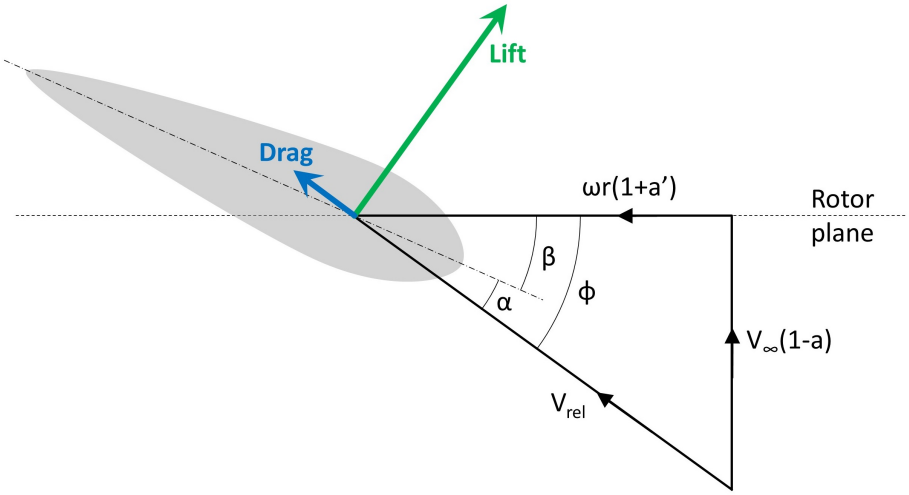

FIGURE 2.5: Inflow velocities, associated angles and aerodynamic forces on a rotating airfoil seen from the tip of the blade.

Once ϕ is known, the angle of attack α is given by

$$\alpha = \phi - \beta, \tag{2.11}$$

where β is the angle of the airfoil with the rotor plane, including structural twist and pitch. The angle of attack α is needed to determine the lift and drag coefficients C_l and C_d, which also depend on the Reynolds number. At this point the aerodynamic forces (lift l and drag d) on the blade section with chord c are known,

$$l = \frac{1}{2}\rho c C_l V_{rel}^2, \tag{2.12}$$

$$d = \frac{1}{2}\rho c C_d V_{rel}^2. \tag{2.13}$$

The inflow angle ϕ is used again to project the lift and drag into load components normal and tangential to the rotor plane,

$$f_n = l\cos\phi + d\sin\phi, \tag{2.14}$$

$$f_t = l\sin\phi - d\cos\phi. \tag{2.15}$$

These loads need to be integrated along the blades. The sum of all normal forces gives the thrust, and the contribution of all tangential forces produces the aerodynamic torque, which relates to the aerodynamic power through the rotor speed ω. If all N blades see the same inflow conditions,

$$T = N\int_0^R f_n dr, \tag{2.16}$$

$$P = N\omega\int_0^R f_t r dr. \tag{2.17}$$

The above equations summarize the basic steady BEM method. Further details can be found in, for example, Hansen [9] and Sørensen [10]. To include unsteady loads and other effects not captured by the method a set of corrections are typically applied:

- Prandtl's tip loss factor corrects the BEM assumption of infinite number of blades.
- Glauert's correction factor is an empirical rectification applied for large values of the axial induction factor, for which the momentum theory is not valid anymore.
- A dynamic inflow model is needed in unsteady calculations to take into account the delay existing between a change in the inflow conditions and a change in the induced velocities.
- A dynamic stall model is applied to capture the delay between a change in angle of attack and a change in local aerodynamic loads.
- If the rotor is yawed or tilted, a yaw/tilt model should be applied to account for the spatial variations of the induced velocities.

Although some limitations of the BEM method are overcome with engineering corrections, a more detailed model is sometimes necessary (e.g. to capture the aeroelastic response of non-straight blades). One option to capture 3-D effects and to physically model the wake is to use potential-flow aerodynamics or vortex methods. For small angles of attack, the flow can be assumed incompressible, irrotational and inviscid. Then the flow past an airfoil can be modelled with a vortex filament of strength Γ, with the lift force given by the Kutta-Joukowski theorem,

$$\vec{l} = \rho \vec{V_\infty} \times \vec{\Gamma}. \tag{2.18}$$

The total lift produced by a 3-D blade can be modelled by a series of vortex filaments (bound vortices) along its span, method known as lifting line theory. In a similar manner, the wake can be modelled with free vortices in the chordwise (trailing vortices) and spanwise (shed vortices) directions. The interaction between vortices is computed via the Biot-Savart law, which provides the velocity $\vec{w}$ induced in a point located at $\vec{r}$ by a vortex filament of strength Γ,

$$\vec{w} = \frac{\Gamma}{4\pi} \oint \frac{\vec{r} \times \vec{ds}}{r^3}, \tag{2.19}$$

where $\vec{ds}$ is a vector along the vortex filament. Further details on potential-flow aerodynamics can be found in, for example, Milne-Thomson [11].

High-fidelity aerodynamic methods are based on CFD, which solves the Navier-Stokes equations numerically. The turbulent scales involved in wind turbine aerodynamics range from kilometers in the atmospheric boundary layer to milimiters in the blade boundary layer, which makes the direct numerical simulation (DNS) impractical [12]. A widely used approximation is the unsteady Reynolds-averaged Navier-Stokes (URANS), which provides a statistical description of the flow by decomposing the flow quantities — velocity and pressure — into a time-averaged term and a fluctuating term. The average part of the Navier-Stokes equations is solved, while the fluctuating (turbulent) part is modelled, usually as an added viscosity. Another approach that has gained attention in recent years is large-eddy simulation (LES), which resolves the large, energy-containing eddies in the flow down to a certain length scale and models the smaller eddies, with the subsequent increase in computational requirements when compared to URANS. Also for reasons of computational cost, in most CFD computations of wind turbines the rotor is not directly modelled due to the fine discretization needed. Instead, the wind turbine is commonly represented by body forces distributed over a disc (actuator disc model), along rotating lines (actuator line model, Sørensen and Shen [13]) or over the blade surface (actuator surface model, Shen et al. [14]). The choice of wind turbine representation in each case depends on the problem size and application. Vortex methods with a lifting line aerodynamic model are also capable of reaching high fidelity levels by resolving the vorticity-formulated Navier-Stokes equations, using what is commonly known as a particle-mesh approach (Ramos-Garcia et al. [15]).

Although CFD models offer a high level of accuracy, the solution is often dependent on the turbulence model and discretization employed, and due to their high computational cost they are usually applied for detailed studies. A comprehensive review of CFD methods for wind turbines is given in, for example, Sanderse et al. [12].

2.2.3 Hydrodynamics

The high Reynolds number of the water flow around an offshore structure makes potential flow a good starting point to model the fluid-structure interaction. Linear or Airy wave theory [16], often used to describe the incident wave field, is based on potential flow and linearized boundary conditions, assuming flat bottom and small wave amplitudes.

Typically formulated in the frequency domain, radiation-diffraction theory (see, for example, Newman [17]) is the most widely used tool to compute hydrodynamic loads on floating bodies. If linearity is assumed, the radiation and diffraction problems can be solved separately: in the radiation problem the body is forced to oscillate with frequency ω in otherwise calm water; and in the diffraction problem the body is fixed and exposed to regular waves with frequency ω and unit amplitude. Invoking linearity once again, the diffraction results for wave amplitude A are simply A times the results for unit amplitude, and the results for irregular waves can be obtained as a linear superposition of the results for different regular waves. Given that potential flow is assumed, the velocity field stems from a velocity potential Φ and the Laplace equation needs to be satisfied in the entire domain,

$$\nabla^2 \Phi = 0. \tag{2.20}$$

Following the coordinate system in Fig. 2.6, the velocity potential for harmonic motion at any point in the fluid domain can be given in complex notation,

$$\Phi(x, y, z, t) = \Re\{\phi e^{i\omega t}\}, \tag{2.21}$$

where $\Re$ indicates the real part, i is the imaginary unit, ω is the incident wave frequency and t is time. The complex velocity potential ϕ is the sum of the diffraction and the radiation potentials. The diffraction potential ϕ_D is due to the velocity potential of the incident wave ϕ_0 and the velocity potential due to wave scattering ϕ_7. The radiation potential ϕ_R is due to the motion of the body in six degrees of freedom $\xi_j = \Re\{\hat{\xi}_j e^{i\omega t}\}$, with $j = 1...6$. Therefore

$$\phi = \phi_D + \phi_R = \phi_0 + \phi_7 + \sum_{j=1}^{6} \hat{\xi}_j \phi_j, \tag{2.22}$$

where ϕ_j is the radiation velocity potential created when the body oscillates with unit amplitude in the j^{th} mode. The total velocity potential must satisfy Eqn. (2.20) in the entire domain as well as the linearized free-surface boundary condition,

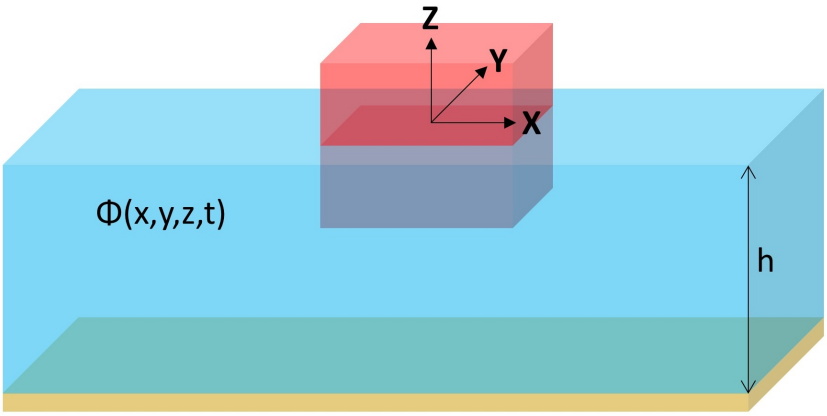

FIGURE 2.6: Coordinate system for the radiation-diffraction problem.

$$\frac{\partial \phi}{\partial z} - \frac{\omega^2}{g}\phi = 0 \quad \text{at} \quad z = 0, \tag{2.23}$$

with g being the gravitational constant. The bottom boundary condition should also be satisfied,

$$\frac{\partial \phi}{\partial z} = 0 \quad \text{at} \quad z = -h, \tag{2.24}$$

where h is the water depth. On the body surface S_B the diffraction potential must satisfy a boundary condition that corresponds to zero normal velocity,

$$\frac{\partial \phi_D}{\partial n} = 0 \quad \Longrightarrow \quad \frac{\partial \phi_0}{\partial n} = -\frac{\partial \phi_7}{\partial n}, \tag{2.25}$$

while the six radiation potentials must satisfy conditions corresponding to the wall velocity in the normal direction,

$$\frac{\partial \phi_j}{\partial n} = i\omega n_j \quad \text{for} \quad j = 1, 2, 3, \tag{2.26}$$

$$\frac{\partial \phi_j}{\partial n} = i\omega(\vec{r} \times \vec{n})_{j-3} \quad \text{for} \quad j = 4, 5, 6. \tag{2.27}$$

Here $\vec{n}$ is the vector normal to the body surface pointing into the body, and $\vec{r} = (x, y, z)$. Finally, the radiation and scattering potentials are caused by the presence of the body, therefore they must vanish as one approaches infinity. This is imposed through the radiation condition at infinity,

$$\phi_j \propto \frac{e^{-ikR}}{\sqrt{R}} \quad \text{as} \quad R \to \infty \quad \text{for} \quad j = 1...7, \tag{2.28}$$

where k is the wave number and $R = \sqrt{x^2 + y^2}$. Once the total velocity potential ϕ is known, the pressure field is given by the linearized Bernoulli equation,

$$p = -\rho \left(\frac{\partial \phi}{\partial t} + gz \right), \tag{2.29}$$

where ρ is the water density. The vector of forces and moments $\mathbf{F}$ is obtained by pressure integration over the body surface S_B,

$$\mathbf{F} = \int_{S_B} p \begin{pmatrix} \vec{n} \\ \vec{r} \times \vec{n} \end{pmatrix} dS. \tag{2.30}$$

The radiation-diffraction problem is usually solved numerically with panel methods, where the number of panels chosen to discretize the body should be a reasonable balance between computational cost and accuracy. The forces and moments obtained with Eqn. (2.30) result in hydrostatic restoring coefficients $\mathbf{C_{hst}}$ (from forces proportional to body displacements), radiation damping coefficients $\mathbf{B}$ (from forces proportional to body velocities), added mass coefficients $\mathbf{A}$ (from forces proportional to body accelerations) and wave excitation coefficients $\mathbf{F_{exc}}$ (from forces depending on the incident waves). These frequency-domain results are normally included in time-domain numerical models through the Cummins equation (see Cummins [18] and Ogilvie [19]), which describes the linearized motion of a freely floating body in waves,

$$(\mathbf{M} + \mathbf{A}_\infty)\ddot{\boldsymbol{\xi}} + \int_0^t \mathbf{K}(t-\tau)\dot{\boldsymbol{\xi}}(\tau)d\tau + \mathbf{C}_{hst}\boldsymbol{\xi} = \mathbf{F}_{exc}. \tag{2.31}$$

Here $\boldsymbol{\xi} = [\xi_1 ... \xi_6]^T$, $\mathbf{M}$ is a mass and inertia matrix, and $\mathbf{A}_\infty$ is the infinite-frequency limit of the frequency-dependent added mass matrix $\mathbf{A}$. The convolution integral represents radiation memory effects where $\mathbf{K}$ is the radiation-retardation kernel, given by the cosine transform of the frequency-dependent radiation damping $\mathbf{B}$,

$$\mathbf{K}(t) = \frac{2}{\pi} \int_0^\infty \mathbf{B}(\omega) \cos(\omega t) d\omega. \tag{2.32}$$

Additional effects can be included in Eqn. (2.31) as external forcing terms on the right-hand side. These effects may include mooring reactions, aerodynamic loads or viscous effects. The latter are not included in the radiation-diffraction analysis due to the assumption of potential flow, and are typically accounted for through the drag term in the Morison equation, linear damping coefficients, quadratic damping coefficients, or a combination of the three. The Morison equation [20] is the most commonly used method to compute hydrodynamic forces on slender cylinders. The horizontal force on a vertical moving cylinder strip with height dz (see Fig. 2.7) is given by

$$dF = \left(\rho A \dot{u} + \rho C_a A (\dot{u} - \ddot{x}) + \frac{1}{2} \rho C_D D (u - \dot{x}) |u - \dot{x}| \right) dz, \tag{2.33}$$

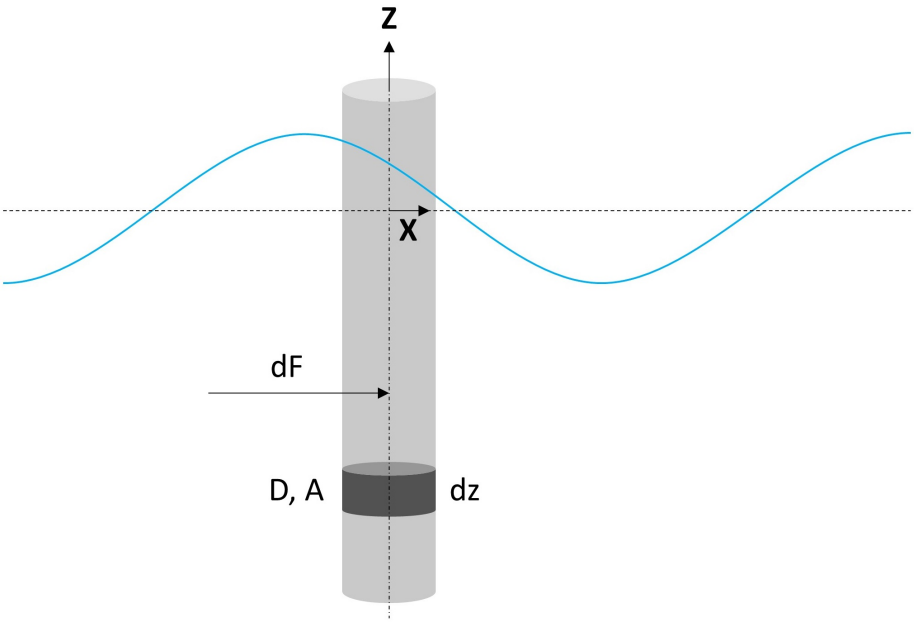

FIGURE 2.7: Morison forcing on a vertical cylinder.

where ρ is the water density, D and A are the diameter and cross-sectional area of the cylinder, u and $\dot{x}$ are the local horizontal particle velocity and body velocity, and dot indicates time derivative, $\dot{u} = \partial u / \partial t$. The drag and added mass coefficients, C_D and C_a, depend on the local flow conditions (namely the Reynolds and Keulegan-Carpenter numbers and the surface roughness) and need to be chosen empirically or with the help of lookup tables. A useful reference to estimate the Morison coefficients is Sumer and Fredsøe [21].

The first term in Eqn. (2.33) is the Froude-Krylov force, which relates to the pressure in the undisturbed wave field. The second term is the hydrodynamic mass force and represents the force needed to accelerate the flow around the cylinder. These two terms are often combined into an inertia term. The last term or viscous drag term represents viscous effects such as skin friction and vortex shedding. For offshore wind support structures the inertia term usually dominates over the drag term, and the order of the model employed to describe the wave kinematics dictates the order of the hydrodynamic forcing. In theory, the applicability of the Morison equation is limited to slender bodies with $D/\lambda \leq 0.2$, where λ is the wave length. For $D/\lambda > 0.2$ the solution by MacCamy and Fuchs [22] may be used to account for wave scattering. The radiation-diffraction theory, on the other hand, covers the whole range of D/λ.

In severe environmental conditions linear methods may not be sufficient to represent the wave-structure interaction, and nonlinear methods should be used instead. In radiation-diffraction theory, second-order effects arise from the interaction of first-order terms and from the second-order velocity potential (see, for example, [23]). These second-order hydrodynamic loads are called difference- and sum-frequency loads, and are associated to the difference and the sum of frequency pairs in the first-order problem.

For slender bodies the Morison formulation may be combined with higher-order representations of the wave kinematics. For irregular sea states, second-order wave kinematics can be computed with, for example, Sharma and Dean's method [24]. A numerical method to compute fully nonlinear wave kinematics has been developed by Engsig-Karup et al. [25]. The latter has been used together with the Morison equation to compute nonlinear wave forces on a floating wind turbine [26, 27, 28]. An extension of the Morison equation (2.33) that includes nonlinear forcing terms (other than the drag term) was proposed by Rainey [29, 30]. According to his formulation (see Fig. 2.8), the horizontal force on a vertical moving cylinder strip with height dz is

$$dF = \left(\rho A \dot{u} + \rho C_a A (\dot{u} - \ddot{x}) + \frac{1}{2} \rho C_D D (u - \dot{x}) |u - \dot{x}| + \rho C_a A \frac{\partial w}{\partial z} (u - \dot{x}) \right) dz, \quad (2.34)$$

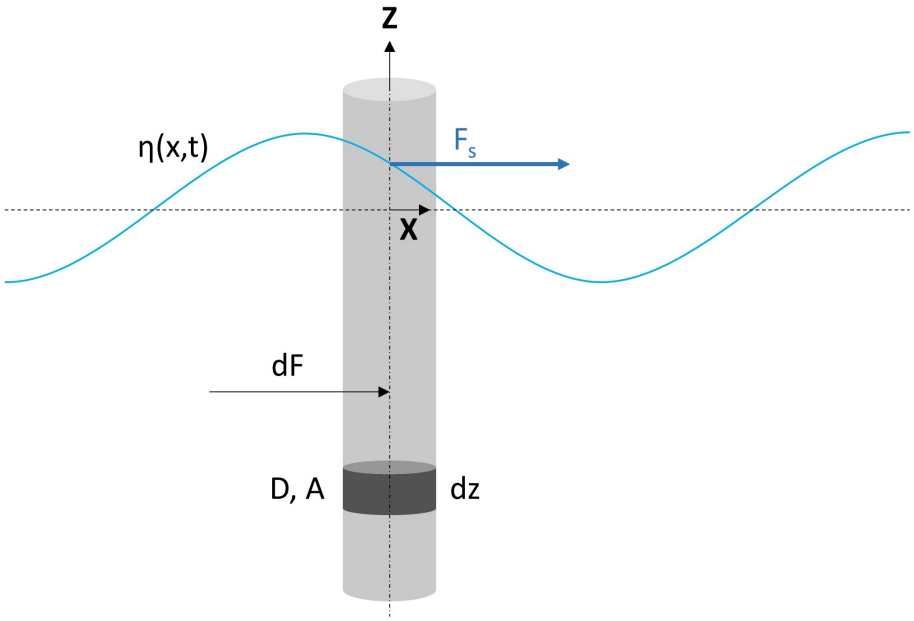

FIGURE 2.8: Rainey forcing on a vertical cylinder.

where w is the local vertical particle velocity. In Rainey's formulation the wave particle acceleration is given by the Lagrangian acceleration, $\dot{u} = \partial u/\partial t + u\partial u/\partial x + w\partial u/\partial z$ in 2-D, as opposed to the Eulerian acceleration used in Eqn. (2.33). The last term in Eqn. (2.34) is called the axial divergence force and accounts for the finite length of the body. In addition, Rainey proposes a point force applied at the intersection between the water surface and the piercing body to account for the change in kinetic energy in the flow,

$$F_s = -\frac{1}{2} \rho C_a A \frac{\partial \eta}{\partial x} (u - \dot{x})^2, \quad (2.35)$$

where η is the free-surface elevation at the center of the cylinder. Fully nonlinear wave kinematics computed with the method presented in [25] have been combined with Rainey forcing on a monopile by Schløer et al. [31, 32, 33].

More advanced hydrodynamic effects such as green water and breaking wave loads can be investigated with CFD, with the consequent increase in computational cost mainly due to the modelling of the free surface and the moving mesh needed to represent the floating body. Hydrodynamics based on CFD has been applied to monopile wind turbines (Paulsen et al. [34], Ghadirian et al. [35]) and floating wind turbines (Nematbakhsh et al. [36, 37], Dunbar et al. [38], Borisade et al. [39], Sarlak et al. [40]).

2.2.4 Mooring dynamics

The main purpose of the mooring system for a floating wind turbine is station keeping. When the structure is displaced from its equilibrium position, the mooring system introduces restoring forces that push the structure towards equilibrium. In the simplest case the mooring system can be modelled as quasi-static, meaning that the restoring forces only depend on the position of the fairleads and that dynamic effects — such as inertial and hydrodynamic loads — are neglected. If such force-displacement relationship is assumed linear it can be written using Hooke's law,

$$\mathbf{F} = -\mathbf{C}\boldsymbol{\xi}, \tag{2.36}$$

where $\mathbf{F}$ is the 6x1 vector of mooring forces and moments, $\boldsymbol{\xi}$ is the 6x1 vector of displacements and $\mathbf{C}$ is the 6x6 mooring restoring matrix. This linear approximation, useful for frequency-domain linear models, assumes small displacements around the equilibrium position. On the other hand, the information on individual mooring line tension is lost, since $\mathbf{F}$ refers to the global mooring forces (i.e. the sum of forces in all lines).

The linear approximation is more appropriate for taut mooring systems, where the restoring force is due to axial strain. For slack mooring systems such as catenaries, the restoring force is mainly due to the change in the amount of line that rests on the seabed. In these cases the nonlinear force-displacement relationship can be captured by solving the nonlinear catenary equations given in, for example, Faltinsen [41]. Consider the inelastic catenary line shown in Fig. 2.9, with a total length L and horizontal and vertical distances between anchor point and fairlead point X and h, respectively. A portion of the cable is resting on the seabed, thus the suspended length is $L_s \leq L$. The nonlinear force-displacement relationship is given by

$$X = L - h\sqrt{1 + \frac{2a}{h}} + a\cosh^{-1}\left(1 + \frac{h}{a}\right), \tag{2.37}$$

where a is the ratio between the horizontal fairlead tension T_H and the weight per length of the cable in water w. The suspended length L_s is given by

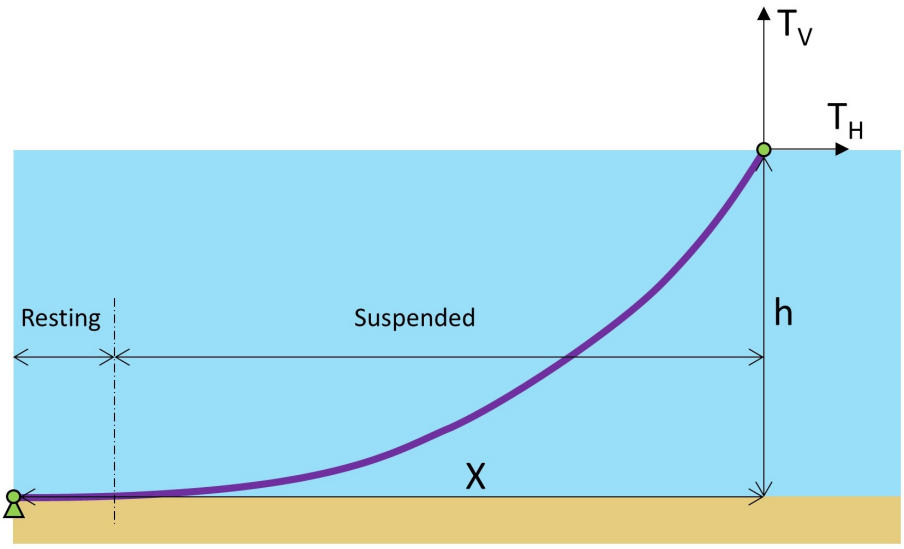

FIGURE 2.9: Inelastic catenary cable in water.

$$L_s = \sqrt{h^2 + 2ha}, \tag{2.38}$$

and the horizontal and vertical components of the fairlead tension are

$$T_H = aw, \tag{2.39}$$
$$T_V = L_s w. \tag{2.40}$$

While quasi-static mooring models are able to predict the line tension and associated response in many cases, dynamic mooring models are needed when extreme events or high-frequency motions occur (Hall et al. [42], Azcona-Armendariz et al. [43]). In dynamic mooring models each line is discretized using a multibody (lumped mass) or FEM approach, and dynamic effects such as inertia, hydrodynamic loads and seabed interaction are typically included. These effects are necessary to capture the mooring line eigenmodes (Nygaard et al. [44]) and to correctly assess fatigue and ultimate mooring loads (Azcona-Armendariz et al. [45]). Some FEM mooring models are also able to capture the propagation of snap loads (see, for example, Palm et al. [46]).

2.2.5 Aero-hydro-servo-elastic numerical tools

Under certain assumptions, frequency-domain numerical tools can combine some of the simplest modelling options to represent the four elements presented above (e.g. rigid body dynamics, actuator point aerodynamics, Morison-based hydrodynamics and linearized mooring stiffness). High-fidelity tools, on the other hand, are able to model with great detail some of the four elements but the others are often

oversimplified for the sake of computational cost (e.g. a model with CFD hydrodynamics will likely represent the structure as a rigid body and neglect aerodynamic loads). A good compromise between accuracy and computational cost in all four elements is offered by aero-hydro-servo-elastic codes, which include interactions of the structure with wind, waves and the wind turbine control system, while considering flexibility in some components (typically blades, tower and mooring lines). They often provide enough global accuracy to capture the most important physical phenomena, while keeping the computational cost within reasonable limits. A brief summary of the most used aero-hydro-servo-elastic tools in floating offshore wind is given in Tab. 2.1 below.

TABLE 2.1: Summary of the most used aero-hydro-servo-elastic tools and their capabilities for the analysis of floating wind turbines, according to the classification provided in Section 2.2.

Code	**Developer**	**Struct.**	**Aerod.**	**Hydrod.**	**Moor.**
FAST v8	NREL	MOD/FEM	BEM	RD/ME	QS/DYN
Bladed	DNV-GL	MOD/FEM	BEM	RD/ME	QS/DYN
HAWC2	DTU	FEM	BEM	RD/ME	QS/DYN
3DFloat	IFE	FEM	BEM	RD/ME	QS/DYN
Flex5	DTU	MOD	BEM	RD/ME	QS
SIMA	SINTEF	FEM	BEM	RD/ME	QS/DYN

In Tab. 2.1 structural modelling can refer to modal[1] (MOD) or finite-element methods (FEM). Aerodynamics are modelled with blade-element momentum (BEM) in all cases. Hydrodynamics options include radiation-diffraction (RD) or Morison equation (ME). Mooring dynamics can refer to quasi-static (QS) or dynamic (DYN). The reader should note that the information in the table is merely orientative and may not be up to date with the latest developments in all codes. Further, Tab. 2.1 refers to standard versions of the codes, though other custom versions exist (e.g. HAWC2 coupled to CFD aerodynamics).

Although the validation of aero-hydro-servo-elastic tools against experimental data is an ongoing effort (see Section 2.3), numerous code-to-code comparisons have been made as well. Probably the best known is the OCX project series, established by the International Energy Agency (IEA) and driven by the National Renewable Energy Laboratory (NREL). The first project in the series, or OC3 project [47] (Offshore Code Comparison Collaboration) took place between 2005 and 2009, with the aim of comparing several aero-hydro-servo-elastic tools applied to a monopile, a tripod and a spar. A follow-up project, the OC4 project (Offshore Code Comparison Collaboration, Continued), ran from 2010 to 2013 with focus on jacket and semisubmersible support structures. The OC5 project (Offshore Code Comparison Collaboration, Continued, with Correlation) between 2014 and 2018 focused on validation of the numerical tools against experimental data, both at laboratory scale (monopile, semisub) and full scale (jacket/tripod).

[1] Flex5 uses deflection shapes, which are not necessarily modal shapes.

2.3 Experimental methods and validation

Physical tests of floating offshore wind turbines serve as a proof-of-concept and provide a reliable benchmark for the validation of simulation tools. Often laboratory-scale tests can capture the most important physical phenomena while requiring less time, resources and risk than full-scale measurements, and allowing control over the environmental conditions. For instance, the Hywind concept was tested in 2005 at 1:47 scale, see Nielsen et al. [48].

As mentioned earlier, a floating wind turbine experiences complex dynamics influenced by wind, waves, structural response and wind turbine control. Thus, recreating these complex conditions in laboratory scale can be a challenging task. For example, it could be difficult to correctly scale the mass and structural properties of the wind turbine including instrumentation. In some cases the optical tracking systems used to measure the floater position are not accurate enough to capture the small motions involved, as it is the case for the roll and pitch of a tension-leg platform (TLP) [49, 50]. Creating laboratory wind conditions that are representative of the atmospheric conditions for a real wind turbine can be a challenge [51]. In addition, the simultaneous preservation of the Froude and Reynolds numbers is not possible. Usually, the Froude number is preserved to ensure a correct hydrodynamic scaling, which leads to reduced Reynolds number and poor aerodynamic performance if the rotor is scaled directly.

These problems can be mitigated in a number of ways. During the DeepCWind consortium tests (see Martin et al. [52], Goupee et al. [53]), Froude scaling and a geometrically-scaled rotor resulted in thrust levels lower than the target, and the desired thrust was matched by increasing the wind speed. In a later campaign (see Kimball et al. [54]), the rotor was redesigned to match the target thrust. A redesigned rotor together with an adjustment of the blade pitch angle has also been used at DTU for a number of test campaigns (Pegalajar-Jurado et al. [49], Bredmose et al. [51], Madsen et al. [50]). It was observed that, while longer blade chords can provide the right mean thrust, they also result in too much aerodynamic damping. In a later campaign at DTU (Borg et al. [55], see Fig. 2.10), two different rotors were tested: one designed to match the steady thrust; and one designed to match the aerodynamic damping.

A hybrid alternative solution to the scaling of aerodynamic loads has gained popularity in recent years. In a hardware-in-the-loop (HIL) approach the physical rotor and wind field are replaced by actuators at the tower top, which apply the aerodynamic loads computed in real time by a numerical model. The actuators can be ducted fans (Azcona-Armendariz et al. [56]), multi-fan systems (Battistella et al. [57]) or a system of wires (Sauder et al. [58], Bachynski et al. [59]). Hybrid HIL approaches also exist where wind tunnel tests are carried out with the physical wind turbine mounted on a robotic foot that emulates the motion of the floater with computed hydrodynamic and mooring loads (Bayati et al. [60]). While hybrid approaches offer an interesting alternative to the classical testing methods and are able to overcome some of the challenges, the numerical models controlling the actuators

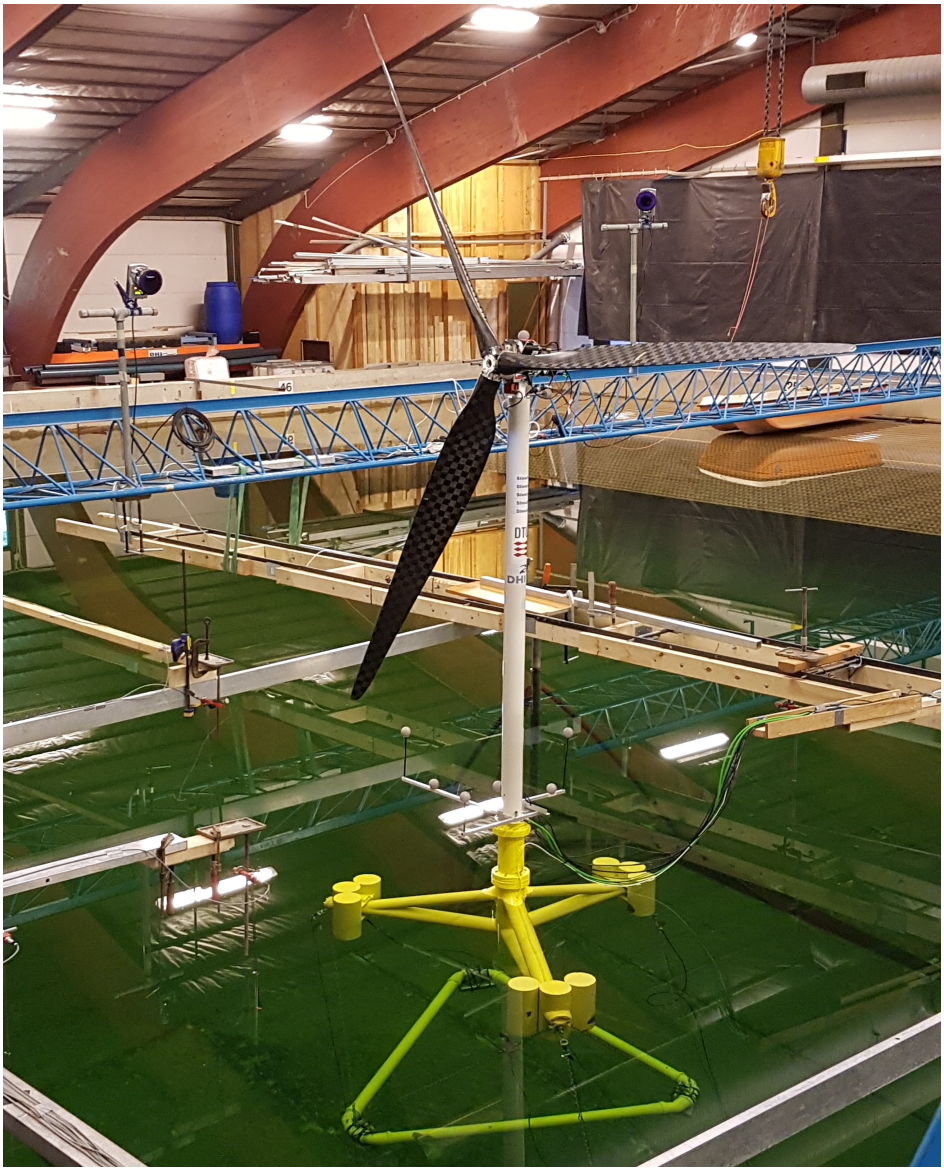

FIGURE 2.10: TetraSpar floating concept in 1:60 scale [55].

need to run faster than real time, which potentially limits their accuracy and their ability to capture all the relevant physics and the interaction phenomena.

One of the main purposes of physical testing of floating wind turbines is the validation of the numerical tools. While several studies have validated numerical models against lab-scale physical tests using different approaches for model calibration (see, for example, Stewart et al. [61], Coulling et al. [62], Browning et al. [63], Pegalajar-Jurado et al. [49], Berthelsen et al. [64]), studies on model validation against full-scale data (Driscoll et al. [65]) are scarce.

References

[1] J. JONKMAN. *Dynamics modeling and loads analysis of an offshore floating wind turbine*. Tech. rep. No. NREL/TP-500-41958, National Renewable Energy Laboratory, 2007.

[2] T.J. LARSEN and T.D. HANSON. "A method to avoid negative damped low frequent tower vibrations for a floating, pitch controlled wind turbine". In: *Journal of Physics: Conference Series* 75.1 (2007).

[3] G. van KUIK and J. PEINKE, eds. *Long-term research challenges in wind energy - A research agenda by the European Academy of Wind Energy*. Springer, 2016.

[4] T.I. FOSSEN. *Handbook of marine craft hydrodynamics and motion control*. 1st. Wiley, 2011.

[5] A. NAESS and T. MOAN. *Stochastic dynamics of marine structures*. 1st. Cambridge University Press, 2013.

[6] R.D. COOK, D.S. MALKUS, and M.E. PLESHA. *Concepts and applications of finite element analysis*. Wiley, 1989.

[7] A.A. SHABANA. *Dynamics of multibody systems*. 2nd. Cambridge University Press, 1998.

[8] H. GLAUERT. "Airplane propellers". In: *Aerodynamic theory*. Ed. by W.F. DURAND. Springer, 1935, pp. 169–360.

[9] M.O.L. HANSEN. *Aerodynamics of wind turbines*. 2nd. Earthscan Publications Ltd., 2008.

[10] J.N. SØRENSEN. "Aerodynamic aspects of wind energy conversion". In: *Annual Review of Fluid Mechanics* 43.1 (2011), pp. 427–448.

[11] L.M. MILNE-THOMSON. *Theoretical aerodynamics*. Macmillan, 1952.

[12] B. SANDERSE, S.P. van der PIJL, and B. KOREN. "Review of computational fluid dynamics for wind turbine wake aerodynamics". In: *Wind Energy* 14.7 (2011), pp. 799–819.

[13] J.N. SØRENSEN and W.Z. SHEN. "Numerical modeling of wind turbine wakes". In: *Journal of Fluids Engineering* 124.2 (2002), pp. 393–399.

[14] W.Z. SHEN, J.N. SØRENSEN, and J.H. ZHANG. "Actuator surface model for wind turbine flow computations". In: *European Wind Energy Conference and Exhibition*. 2007.

[15] N. RAMOS-GARCÍA, H.J. SPIETZ, J.N. SØRENSEN, and J.H. WALTHER. "Vortex simulations of wind turbines operating in atmospheric conditions using a prescribed velocity-vorticity boundary layer model". In: *Wind Energy* 21.11 (2018), pp. 1216–1231.

[16] G.B. AIRY. *Tides and waves*. 1845.

[17] J.N. NEWMAN. *Marine hydrodynamics*. 1st. The MIT Press, 1977.

[18] W.E. CUMMINS. "The impulse response functions and ship motions". In: *Schiffstechnik* 9 (1962), pp. 101–109.

[19] T.F. OGILVIE. "Recent progress toward the understanding and prediction of ship motions". In: *Fifth Symposium on Naval Hydrodynamics*. 1964, pp. 3–128.
[20] J.R. MORISON, J.W. JOHNSON, and S.A. SCHAAF. "The force exerted by surface waves on piles". In: *Journal of Petroleum Technology* 2.05 (1950), pp. 149–154.
[21] B.M. SUMER and J. FREDSØE. *Hydrodynamics around cylindrical structures*. Revised. World Scientific Publishing Company, 2006.
[22] R.C. MACCAMY and R.A. FUCHS. *Wave forces on piles: a diffraction theory*. Tech. rep. No. 69, Beach Erosion Board, U.S. Army Corps of Engineers, 1954.
[23] J.N. NEWMAN. "Second-order, slowly-varying forces on vessels in irregular waves". In: *Proceedings of the Symposium on the Dynamics of Marine Vehicles and Structures in Waves*. London, 1974, pp. 182–186.
[24] J.N. SHARMA and R.G. DEAN. "Second-order directional seas and associated wave forces". In: *Society of Petroleum Engineers Journal* 21.1 (1981), pp. 129–140.
[25] A.P. ENGSIG-KARUP, H.B. BINGHAM, and O. LINDBERG. "An efficient flexible-order model for 3D nonlinear water waves". In: *Journal of Computational Physics* 228.6 (2009), pp. 2100–2118.
[26] H. BREDMOSE. *Contribution to INNWIND.EU deliverable 4.21: Nonlinear wave loads on a TLP floating wind turbine*. Tech. rep. DTU Wind Energy, 2013.
[27] M. DUPONT and M. AUBRION. *Nonlinear wave forcing on a floating wind turbine. MSc thesis, DTU*. 2014.
[28] A. PEGALAJAR-JURADO, M. BORG, A. ROBERTSON, J. JONKMAN, and H. BREDMOSE. "Effect of second-order and fully nonlinear wave kinematics on a tension-leg-platform wind turbine in extreme wave conditions". In: *Proceedings of the ASME 36th International Conference on Ocean, Offshore and Arctic Engineering (OMAE 2017)*. 2017.
[29] R.C.T. RAINEY. "A new equation for calculating wave loads on offshore structures". In: *Journal of Fluid Mechanics* 204.1 (1989), pp. 295–324.
[30] R.C.T. RAINEY. "Slender-body expressions for the wave load on offshore structures". In: *Proceedings of the Royal Society A: Mathematical, Physical and Engineering Sciences* 450.1939 (1995), pp. 391–416.
[31] S. SCHLØER, H. BREDMOSE, H.B. BINGHAM, and T.J. LARSEN. "Effects from fully nonlinear irregular wave forcing on the fatigue life of an offshore wind turbine and its monopile foundation". In: *Proceedings of the ASME 31st International Conference on Ocean, Offshore and Arctic Engineering (OMAE 2012)*. 2012.
[32] S. SCHLØER. "Fatigue and extreme wave loads on bottom fixed offshore wind turbines". PhD thesis. DTU, 2013.
[33] S. SCHLØER, H. BREDMOSE, and H.B. BINGHAM. "The influence of fully nonlinear wave forces on aero-hydro-elastic calculations of monopile wind turbines". In: *Marine Structures* 50 (2016), pp. 162–188.
[34] B.T. PAULSEN, H. BREDMOSE, H.B. BINGHAM, and N.G. JACOBSEN. "Forcing of a bottom-mounted circular cylinder by steep regular water waves at finite depth". In: *Journal of Fluid Mechanics* 755 (2014), pp. 1–34.
[35] A. GHADIRIAN, H. BREDMOSE, and M. DIXEN. "Breaking phase focused wave group loads on offshore wind turbine monopiles". In: *Journal of Physics: Conference Series* 753.9 (2016).

[36] A. NEMATBAKHSH, D.J. OLINGER, and G. TRYGGVASON. "Nonlinear simulation of a spar buoy floating wind turbine under extreme ocean conditions". In: *Journal of Renewable and Sustainable Energy* 6.3 (2014).

[37] A. NEMATBAKHSH, E.E. BACHYNSKI, Z. GAO, and T. MOAN. "Comparison of wave load effects on a TLP wind turbine by using computational fluid dynamics and potential flow theory approaches". In: *Applied Ocean Research* 53 (2015), pp. 142–154.

[38] A.J. DUNBAR, B.A. CRAVEN, and E.G. PATERSON. "Development and validation of a tightly coupled CFD/6-DOF solver for simulating floating offshore wind turbine platforms". In: *Ocean Engineering* 110 (2015), pp. 98–105.

[39] F. BORISADE, T. CHOISNET, and P.W. CHENG. "Design study and full scale MBS-CFD simulation of the IDEOL floating offshore wind turbine foundation". In: *Journal of Physics: Conference Series* 753.9 (2016).

[40] H. SARLAK, A. PEGALAJAR-JURADO, and H. BREDMOSE. "CFD simulations of a newly developed floating offshore wind turbine platform using OpenFOAM". In: *Proceedings of the 21st Australasian Fluid Mechanics Conference*. 2018.

[41] O.M. FALTINSEN. *Sea loads on ships and offshore structures*. 1st. Cambridge University Press, 1990.

[42] M. HALL, B. BUCKHAM, and C. CRAWFORD. "Evaluating the importance of mooring line model fidelity in floating offshore wind turbine simulations". In: *Wind Energy* 17.12 (2014), pp. 1835–1853.

[43] J. AZCONA-ARMENDARIZ, X. MUNDUATE, L. GONZÁLEZ, and T.A. NYGAARD. "Experimental validation of a dynamic mooring lines code with tension and motion measurements of a submerged chain". In: *Ocean Engineering* 129 (2017), pp. 415–427.

[44] T.A. NYGAARD, J. de VAAL, M.H. MADSEN, H. ANDERSEN, and J. ALTUZARRA. "Catenary mooring chain eigenmodes and the effects on fatigue life". In: *Oral presentation at the EERA DeepWind 2018 conference*. Trondheim, Norway, 2018.

[45] J. AZCONA-ARMENDARIZ, D. PALACIO, X. MUNDUATE, L. GONZÁLEZ, and T.A. NYGAARD. "Impact of mooring lines dynamics on the fatigue and ultimate loads of three offshore floating wind turbines computed with IEC 61400-3 guideline". In: *Wind Energy* 20.5 (2017), pp. 797–813.

[46] J. PALM, C. ESKILSSON, and L. BERGDAHL. "An hp-adaptive discontinuous Galerkin method for modelling snap loads in mooring cables". In: *Ocean Engineering* 144 (2017), pp. 266–276.

[47] J. JONKMAN and W. MUSIAL. *Offshore Code Comparison Collaboration (OC3) for IEA Task 23: Offshore wind technology and deployment*. Tech. rep. No. NREL/TP-5000-48191, National Renewable Energy Laboratory, 2010.

[48] F.G. NIELSEN, T.D. HANSON, and B. SKAARE. "Integrated dynamic analysis of floating offshore wind turbines". In: *Proceedings of the ASME 25th International Conference on Ocean, Offshore and Arctic Engineering (OMAE 2006)*. 2006.

[49] A. PEGALAJAR-JURADO, A.M. HANSEN, R. LAUGESEN, R.F. MIKKELSEN, M. BORG, T. KIM, N.F. HEILSKOV, and H. BREDMOSE. "Experimental and

numerical study of a 10MW TLP wind turbine in waves and wind". In: *Journal of Physics: Conference Series* 753.9 (2016).

[50] F.J. MADSEN, T.R.L. NIELSEN, T. KIM, M. BORG, H. BREDMOSE, A. PEGALAJAR-JURADO, R.F. MIKKELSEN, M. MIRZAEI, A.K. LOMHOLT, and P. SHIN. "Experimental and numerical response analysis of the scaled DTU 10MW TLP floating wind turbine with different control strategies". In: *Renewable Energy (in review)* (2019).

[51] H. BREDMOSE, F. LEMMER, M. BORG, A. PEGALAJAR-JURADO, R.F. MIKKELSEN, T.S. LARSEN, T. FJELSTRUP, W. YU, A.K. LOMHOLT, L. BOEHM, and J. AZCONA-ARMENDARIZ. "The Triple Spar campaign: Model tests of a 10MW floating wind turbine with waves, wind and pitch control". In: *Energy Procedia* 137 (2017), pp. 58–76.

[52] H.R. MARTIN, R. KIMBALL, A.M. VISELLI, and A.J. GOUPEE. "Methodology for wind/wave basin testing of floating offshore wind turbines". In: *Journal of Offshore Mechanics and Arctic Engineering* 136.2 (2014).

[53] A.J. GOUPEE, B.J. KOO, R. KIMBALL, K.F. LAMBRAKOS, and H.J. DAGHER. "Experimental comparison of three floating wind turbine concepts". In: *Journal of Offshore Mechanics and Arctic Engineering* 136.2 (2014).

[54] R. KIMBALL, A.J. GOUPEE, M.J. FOWLER, E.J. de RIDDER, and J. HELDER. "Wind/wave basin verification of a performance-matched scale-model wind turbine on a floating offshore wind turbine platform". In: *Proceedings of the ASME 33rd International Conference on Ocean, Offshore and Arctic Engineering (OMAE 2014)*. 2014.

[55] M. BORG, H. BREDMOSE, H. STIESDAL, A. PEGALAJAR-JURADO, F.J. MADSEN, T.R.L. NIELSEN, R.F. MIKKELSEN, M. MIRZAEI, and A.K. LOMHOLT. "Physical model testing of the TetraSpar floater in two configurations. Part I: Experimental setup and hydrodynamic analysis". In: *Marine Structures (in review)* (2018).

[56] J. AZCONA-ARMENDARIZ, F. BOUCHOTROUCH, M. GONZALEZ, J. GARCIANDIA, X. MUNDUATE, F. KELBERLAU, and T.A. NYGAARD. "Aerodynamic thrust modelling in wave tank tests of offshore floating wind turbines using a ducted fan". In: *Journal of Physics: Conference Series* 524 (2014).

[57] T. BATTISTELLA, D. de los DOLORES, A. MESEGUER, and R. GUANCHE. "High-fidelity simulation of multi-MW rotor aerodynamics by using a multi-fan". In: *Proceedings of the ASME 37th International Conference on Ocean, Offshore and Arctic Engineering (OMAE 2018)*. 2018.

[58] T. SAUDER, V. CHABAUD, M. THYS, E.E. BACHYNSKI, and L.O. SÆTHER. "Real-time hybrid model testing of a braceless semi-submersible wind turbine. Part I: the hybrid approach". In: *Proceedings of the ASME 35th International Conference on Ocean, Offshore and Arctic Engineering (OMAE 2016)*. 2016.

[59] E.E. BACHYNSKI, M. THYS, T. SAUDER, V. CHABAUD, and L.O. SÆTHER. "Real-time hybrid model testing of a braceless semi-submersible wind turbine. Part II: experimental results". In: *Proceedings of the ASME 35th International Conference on Ocean, Offshore and Arctic Engineering (OMAE 2016)*. 2016.

[60] I. BAYATI, A. FACCHINETTI, A. FONTANELLA, H. GIBERTI, and M. BELLOLI. "A wind tunnel/HIL setup for integrated tests of floating offshore wind turbines". In: *Journal of Physics: Conference Series* 1037.5 (2018), p. 052025.

[61] G. STEWART, M. LACKNER, and A. ROBERTSON. "Calibration and validation of a FAST floating wind turbine model of the DeepCwind scaled tension-leg platform". In: *Proceedings of the 22nd International Offshore and Polar Engineering Conference (ISOPE 2012)*. 2012.

[62] A.J. COULLING, A.J. GOUPEE, A. ROBERTSON, J. JONKMAN, and H.J. DAGHER. "Validation of a FAST semi-submersible floating wind turbine numerical model with DeepCwind test data". In: *Journal of Renewable and Sustainable Energy* 5.2 (2013).

[63] J.R. BROWNING, J. JONKMAN, A. ROBERTSON, and A.J. GOUPEE. "Calibration and validation of a spar-type floating offshore wind turbine model using the FAST dynamic simulation tool". In: *Journal of Physics: Conference Series* 555 (2014).

[64] P.A. BERTHELSEN, E.E. BACHYNSKI, M. KARIMIRAD, and M. THYS. "Real-time hybrid model testing of a braceless semi-submersible wind turbine. Part III: calibration of a numerical model". In: *Proceedings of the ASME 35th International Conference on Ocean, Offshore and Arctic Engineering (OMAE 2016)*. 2016.

[65] F. DRISCOLL, J. JONKMAN, A. ROBERTSON, S. SIRNIVAS, B. SKAARE, and F.G. NIELSEN. "Validation of a FAST model of the Statoil-Hywind Demo floating wind turbine". In: *Energy Procedia* 94 (2016), pp. 3–19.

Chapter 3

About Part II of this thesis

In Part II, three scientific papers related to cascaded modelling of floating offshore wind turbines are included. The relation of each paper with the cascade of models presented in Chapter 2 is shown in Fig. 3.1. In Paper 1 a state-of-the-art numerical model is set up and demonstrated in a wide range of environmental conditions with wind and waves. Paper 2 presents a simplified, efficient frequency-domain tool for the assessment of loads and response to wind and waves in the preliminary phase of floater design. In Paper 3 a time-domain model is established and used to investigate the response of floating wind turbines to waves by comparing to experimental results.

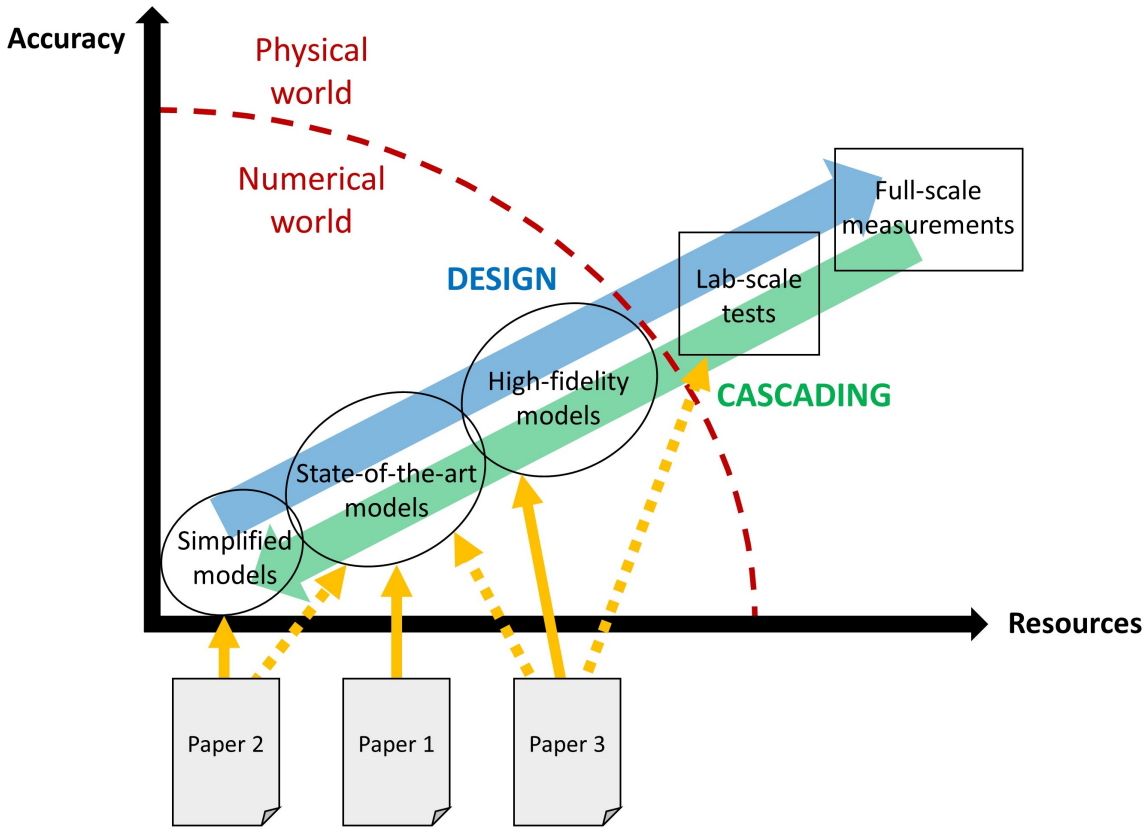

FIGURE 3.1: Overview of papers in the cascade of models.

Paper 1

Title & authors

"State-of-the-art model for the LIFES50+ OO-Star Wind Floater Semi 10MW floating wind turbine", accepted for publication in *Journal of Physics: Conference Series*, 2018. Antonio Pegalajar-Jurado, Henrik Bredmose, Michael Borg, Jonas G. Straume, Trond Landbø, Håkon S. Andersen, Wei Yu, Kolja Müller and Frank Lemmer.

Summary

In this paper the implementation of a state-of-the-art model for the OO-Star Wind Floater Semi 10MW concept is described. The focus is on the hydrodynamic modelling (including viscous effects on the pontoon and heave plates) and on the tower modelling. The model is used to simulate a set of load cases with waves, wind and control.

The response to wind and waves and the controller operation are found adequate for all environmental conditions. For wind speeds above rated and no waves, the surge motion is observed to be only lightly damped due to the controller. Some differences are found in both tower frequency and the dominant tower bending mode when compared to a fully-flexible model.

The model is based on one of the first realistic floating wind turbines in the 10MW class. It is freely available for public use, thus aiding research both in the LIFES50+ project and in the scientific community.

Paper 2

Title & authors

"An efficient frequency-domain model for quick load analysis of floating offshore wind turbines", accepted for publication in *Wind Energy Science*, 2018. Antonio Pegalajar-Jurado, Michael Borg and Henrik Bredmose.

Summary

This paper presents a frequency-domain model that incorporates the main planar degrees of freedom of the floater, as well as tower bending. The model is cascaded from the state-of-the-art model in Paper 1. It includes aerodynamic damping extracted from aeroelastic simulations for each degree of freedom, and approximated hydrodynamic damping.

A general good match to the state-of-the-art model is obtained in wind and waves. The main reasons for deviations are identified and they come from: i) missing viscous forcing in large sea states; ii) the complexity of aerodynamic loads around rated wind speed due to the controller; and iii) underprediction of the tower response.

The model captures the dominant physics and runs 1300-2700 times faster than real time. It allows an efficient exploration of the design space in the first stages of floater design, and facilitates automatic optimization in the floater design process.

Paper 3

Title & authors

"Reproduction of slow-drift motions of a floating wind turbine using second-order hydrodynamics and Operational Modal Analysis", submitted to *Marine Structures*, 2018. Antonio Pegalajar-Jurado and Henrik Bredmose.

Summary

In this paper, a time-domain model with second-order inviscid loads and viscous loads is developed and compared to experimental data. The damping is identified from the test data through Operational Modal Analysis (OMA). The model is specifically built to retain a linear response format and the associated computational efficiency.

The damping levels are found to depend on the sea state. They are acceptably predicted by OMA for mild sea states, while they deviate from the calibrated values for larger sea states. The model generally captures well the response after proper calibration of the damping. For larger sea states, the response in some degrees of freedom is underpredicted due to missing second-order excitation loads.

This study is the first to combine second-order hydrodynamics and OMA in the validation of a numerical model. The linear response format enables efficient computation of the response, once the second-order quadratic transfer functions are available.

Part II

Papers

The actual papers are not included in this online version due to Copyright reasons, but they can be found in the links below:

Paper 1

https://iopscience.iop.org/article/10.1088/1742-6596/1104/1/012024

Paper 2

https://www.wind-energ-sci.net/3/693/2018/wes-3-693-2018.html

Paper 3

https://www.sciencedirect.com/science/article/pii/S095183391830371X

Technical University of Denmark
Department of Wind Energy
Frederiksborgvej 399
Building 118
4000 Roskilde
Denmark
Telephone 46 77 50 85

info@vindenergi.dtu.dk
www.vindenergi.dtu.dk